Current noise and photon noise in quantum cascade lasers

Farhan Rana and Rajeev J. Ram

Research Laboratory for Electronics, Massachusetts Institute of Technology, Cambridge, Massachusetts 02139
(Received 14 August 2001; published 12 March 2002)

A model for the photon noise and the current noise in quantum cascade lasers is presented. It is shown that compared to diode lasers quantum cascade lasers exhibit much less photon-number squeezing even when the noise in the drive current is suppressed well below the shot-noise value. The theoretical model presented in this paper self-consistently accounts for the suppression of the current noise in electron transport in multiple quantum-well structures due to various electronic correlations. The nature of these electronic correlations is discussed. Mechanisms that make photon-number squeezing difficult to achieve in quantum cascade lasers are discussed. Scaling of the laser intensity noise and the current noise with the number of cascaded gain stages is also described. Direct-current modulation response of quantum cascade lasers is also studied, and it is shown that contrary to the predictions in the literature of terahertz modulation bandwidth for these lasers, bandwidth of almost all quantum cascade lasers that have been reported in the literature is limited by the inverse photon lifetime inside the laser cavity to tens of gigahertz.

I. INTRODUCTION

Unipolar quantum cascade lasers (QCL's) utilizing inter-subband transitions to generate photons have become important sources of light in the mid-infrared region (5 μm–15 μm). In this paper a model for the photon noise in QCL's is reported. Current noise associated with electron transport through the active regions is also studied and its effect on the photon noise is evaluated.

QCL's are different from interband semiconductor diode lasers in three important ways that can have a significant impact on their noise properties.

(1) Electron transport in QCL's takes place by tunneling between states in adjacent quantum wells. It is well known that electronic correlations in resonant tunneling in quantum well structures can suppress (or enhance) current noise by providing a negative (or positive) feedback.[1–3] High-impedance suppression of the current noise in semiconductor diode lasers results in light output with squeezed photon-number fluctuations.[4] It is, therefore, intriguing whether suppression of the current noise can also lead to squeezing in QCL's. Any model for the photon noise in QCL's must take into account these electronic correlations self-consistently.

(2) In diode lasers the carrier density in the energy level involved in the lasing action does not increase beyond its threshold value and, therefore, the noise contributed by the nonradiative recombination and generation processes also remains unchanged beyond threshold. In QCL's the electron densities in the upper and lower lasing states do not clamp at threshold, and keep increasing when the bias current is increased beyond threshold. As a result, nonradiative processes contribute significantly to photon noise even at high bias currents.

(3) Since all the gain sections in a QCL are connected electrically and optically, electron-density fluctuations and photon-emission events in different gain sections become correlated. The effect of these correlations on the photon noise in interband cascade lasers has already been discussed in detail,[5,6] and it is the aim of this paper to investigate the role of these correlations in QCL's.

II. OUTLINE

In Sec. IV the nonlinear rate equations for the electron and photon densities in QCL's are presented. The steady-state solution of these rate equations below and above threshold are described. In Sec. V the nonlinear rate equations are linearized to obtain Langevin rate equations for the fluctuations in the electron and photon densities. Electron transport in the multiple quantum-well structure of QCL's is discussed in detail, and a self-consistent model for the fluctuations in the electron-charge densities and the electron-current density is presented. It is shown that a self-consistent description of the fluctuations in the charge and current densities can be carried out in terms of a few device parameters. Langevin noise sources are also used to model the noise associated with electron transport by tunneling. Section V is the main part of this paper. In Sec. VI the set of coupled linearized Langevin rate equations for the fluctuations in the electron densities in different levels of all the cascaded gain stages and the fluctuations in the photon density are solved under the constraints imposed by the biasing electrical circuit. In addition, the direct-current modulation response of QCL's is also evaluated and the maximum possible modulation bandwidth is discussed. The analytical and numerical results on the current noise and the photon noise in QCL's are presented and discussed in Secs. VII and VIII, respectively. In these sections the results obtained are compared with the current and photon noise in interband semiconductor diode lasers. Readers not familiar with the results on the current and photon noise in diode lasers are encouraged to read Appendix F in which a detailed model for the noise in diode lasers is presented.

III. TYPES OF QUANTUM CASCADE LASERS

Many different types of QCL structures have been reported in the literature.[7–19] Almost all of these QCL struc-
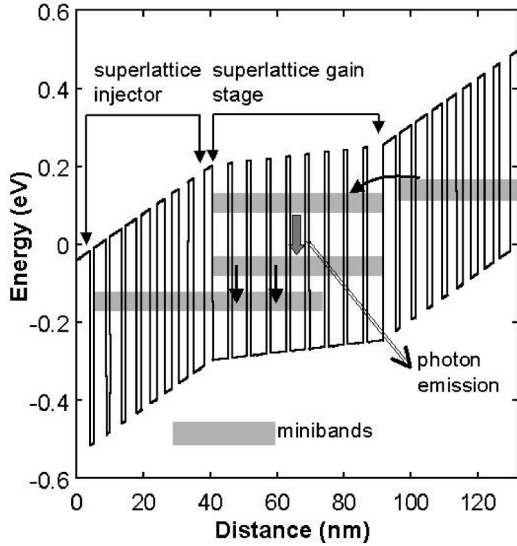
FIG. 1. Superlattice quantum cascade laser.

tures can be classified into two categories:

(1) *Superlattice QCL's* in which the gain stage consists of a superlattice structure and the photons are emitted when the electrons make transitions between two minibands of this superlattice. These minibands are actually clusters of closely spaced energy levels (Fig. 1).[16–19]

(2) *Multiple quantum-well QCL's* in which the gain stage consists of multiple quantum wells (typically two or three) and the radiative electronic transitions occur between two discrete energy levels (Fig. 2).[7–12]

In both types of QCL's, two successive gain stages are separated usually by a superlattice structure known as the *injector*. The superlattice injector has a minigap that prevents the electrons from tunneling out into the injector from the upper energy level(s) of the previous gain stage and, therefore, increases the radiative efficiency. Electrons from the lower energy level(s) of a gain stage can tunnel into the injector, and the injector injects these electrons into the upper
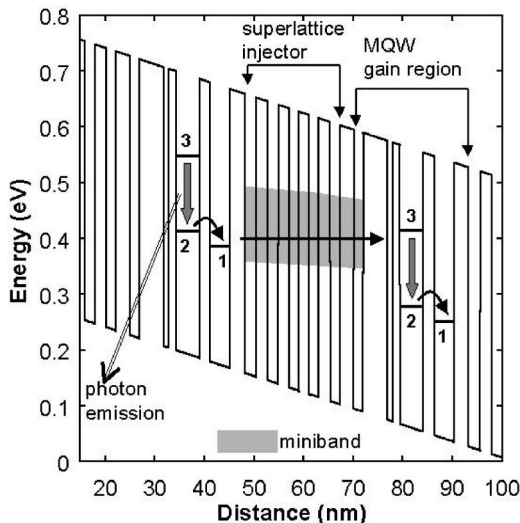
energy level(s) of the next gain stage.

In this paper, photon noise and current noise in only multiple quantum-well QCL's is discussed. The methods presented in this paper are fairly general and can be used to analyze noise and dynamics in a wide variety of QCL's including those with superlattice gain stages. We have chosen to focus on the QCL structure shown in Fig. 2. The operation of this QCL is as follows. Electrons tunnel from the energy states in the superlattice injector into level 3 of the gain stage. Photons are emitted when electrons make radiative transitions from level 3 to level 2. Transitions from level 2 to level 1 occur primarily by emission of optical phonons. Electrons leave the gain stage from level 1 by tunneling out into the superlattice injector of the next stage. In addition, electrons also make nonradiative transitions from level 3 to levels 2 and 1. In this paper we will linearize the nonlinear laser rate equations around a stable operating point to study the noise. The QCL structure we study is fairly general in the sense that the linearized dynamics of many different multiple quantum-well QCL's can be described by a three-level system with an injector state, or with an even simpler model. Therefore, with minor adjustments the model presented here can be used to study different multiple quantum-well QCL structures that have been reported in the literature. For example, in the multiple quantum-well QCL structure employing diagonal radiative electron transitions described in Ref. 20 level 3 is the same as the injector state, and level 1 is the same as the injector state of the next gain stage. The linearized dynamics of the QCL in Ref. 20 can be captured in the model we present in this paper if the transition rates from the injector state into level 3 and from level 1 into the injector state of the next gain stage are made very fast.

IV. RATE EQUATIONS AND STEADY-STATE SOLUTIONS

For the multiple quantum-well QCL structure shown in Fig. 2 the nonlinear rate equations for the electron and photon densities are as follows,

$$\frac{dn_3^j}{dt} = \frac{J_{in}^j}{q} - R_{32}(n_3^j, n_2^j) - R_{31}(n_3^j, n_1^j)$$

$$- \Gamma^j v_g g(n_3^j, n_2^j)\left(S_p + \frac{n_{sp}}{WL}\right), \quad (1)$$

$$\frac{dn_2^j}{dt} = R_{32}(n_3^j, n_2^j) - R_{21}(n_2^j, n_1^j) + \Gamma^j v_g g(n_3^j, n_2^j)\left(S_p + \frac{n_{sp}}{WL}\right), \quad (2)$$

$$\frac{dn_1^j}{dt} = R_{31}(n_3^j, n_2^j) + R_{21}(n_2^j, n_1^j) - \frac{J_{out}^j}{q}, \quad (3)$$

$$\frac{dS_p}{dt} = \sum_{j=1}^{N} \Gamma^j v_g g(n_3^j, n_2^j)\left(S_p + \frac{n_{sp}}{WL}\right) - \frac{S_p}{\tau_p}, \quad (4)$$

$$P_{out} = \eta_o h\nu \frac{WLS_p}{\tau_p}. \quad (5)$$

FIG. 2. Multiple quantum-well quantum cascade laser.

In the above equations, n_k^j is the electron density (cm^{-2}) in the kth energy level of the jth gain stage. J_{in}^j and J_{out}^j are the electron-current densities (cm^{-2}) tunneling into level 3 and tunneling out of level 1 of the jth gain stage, respectively. Only in steady state J_{in}^j equals J_{out}^j. S_p is the photon density (cm^{-2}) inside the optical cavity. S_p is equal to the total number of photons inside the cavity divided by the width W and the length L of the cavity. v_g is the group velocity of the lasing mode and g is the optical gain (cm^{-1}) contributed by a single gain stage. Γ^j is the mode-confinement factor for the jth gain stage. N is the total number of cascaded gain stages. R_{32} is the net transition rate from level 3 to level 2 through nonradiative processes and spontaneous emission into the nonlasing modes. Similarly, R_{31} and R_{21} are the net transition rates from level 3 and level 2 into level 1, respectively. n_{sp} is the spontaneous emission factor.[21] P_{out} is the output power from the laser. η_o is the power output coupling efficiency and τ_p is the photon lifetime inside the cavity. The expression for τ_p is,

$$\frac{1}{\tau_p} = v_g(\alpha_i + \alpha_m) = v_g\left[\alpha_i + \frac{1}{L}\ln\left(\frac{1}{\sqrt{r_1 r_2}}\right)\right], \quad (6)$$

where α_i is the internal loss of the cavity, α_m is the loss from the cavity facets, and r_1 and r_2 are the facet reflectivities. The power output coupling efficiency η_o from the facet with reflectivity r_1 is

$$\eta_o = \frac{(1-r_1)\sqrt{r_2}}{[(1-r_1)\sqrt{r_2} + (1-r_2)\sqrt{r_1}]} \frac{\alpha_m}{(\alpha_m + \alpha_i)}. \quad (7)$$

For simplicity it is assumed that all the gain stages have the same mode-confinement factor, i.e., $\Gamma^j = \Gamma$ for all j. This assumption is valid if all the cascaded gain stages are located close to the peak of the transverse profile of the optical mode where the field strength varies slowly. Even for QCL's with large number of gain stages numerical simulations show that corrections to the solution obtained by assuming all Γ^j to be equal are small. Under this assumption, the steady-state electron densities n_k^j are the same in all the gain stages, and the index j may be suppressed when calculating the steady-state electron densities.

Steady-state solutions

Below threshold

The steady-state solution to the rate equations can be found by setting all the time derivatives equal to zero and putting $J_{in} = J$. Below threshold, steady-state carrier densities can be found by putting $S_p = 0$ and solving the equations (the index j has been suppressed)

$$R_{32}(n_3, n_2) + R_{31}(n_3, n_1) = \frac{J}{q}, \quad (8)$$

$$R_{32}(n_3, n_2) = R_{21}(n_2, n_1). \quad (9)$$

The third equation can be obtained by realizing that J_{out} is also a function of n_1
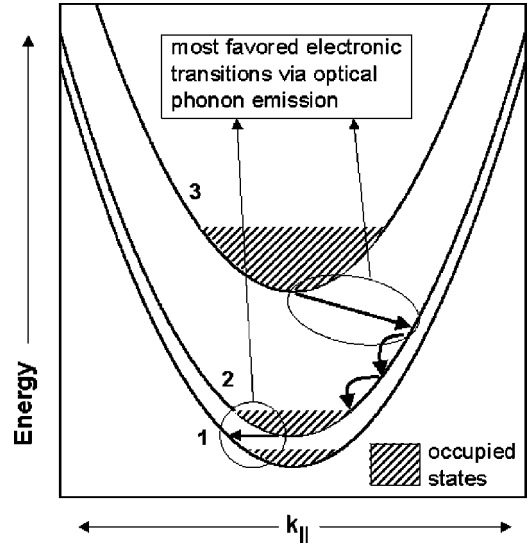

FIG. 3. Energy subbands of the three levels of the gain stage. Most favored electronic transitions by optical phonon emission are almost horizontal in the $E(\vec{k})$-$\vec{k}$ space.

$$J_{out}(n_1) = J. \quad (10)$$

To proceed further, analytical expressions for the transition rates are required. These transition rates can be approximated as

$$R_{32}(n_3, n_2) \cong \frac{n_3}{\tau_{32}}, \quad (11)$$

$$R_{31}(n_3, n_1) \cong \frac{n_3}{\tau_{31}}, \quad (12)$$

$$R_{21}(n_2, n_1) \cong \frac{n_2}{\tau_{21}}, \quad (13)$$

$$\frac{J_{out}(n_1)}{q} \cong \frac{n_1}{\tau_{out}}. \quad (14)$$

The rationale for the approximations in Eqs. (11)–(13) is that optical phonons are largely responsible for intersubband transitions. As shown in Fig. 3, optical phonon mediated intersubband transitions that are almost horizontal in $E(\vec{k})$-$\vec{k}$ plane are more likely to occur.[22] Therefore, the transitions rates from an upper to a lower subband are not much affected by the electron density in the lower subband, as long as the electron density in the lower subband is small. More complicated expressions for these transition rates, such as,

$$R_{qk}(n_q, n_k) = \frac{n_q}{\tau_{qk}} - \frac{n_k}{\tau_{kq}} \quad (15)$$

may be used if necessary.

The expression for J_{out} in Eq. (14) does not depend on the electron density in the injector since electrons in the injector states are assumed to relax very quickly into the ground state of the injector that is spatially localized near the next gain

stage. Using Eqs. (11)–(14) in Eqs. (8)–(10), expressions for the carrier densities can be obtained as a function of the current density,

$$n_3 = \frac{J}{q} \frac{\tau_{32}\tau_{31}}{\tau_{32}+\tau_{31}}, \tag{16}$$

$$n_2 = \frac{J}{q} \frac{\tau_{21}\tau_{31}}{\tau_{32}+\tau_{31}}, \tag{17}$$

$$n_1 = \frac{J}{q} \tau_{out}. \tag{18}$$

Above threshold

Above threshold, the gain is clamped to a value determined by equating the gain with the loss

$$\sum_{j=1}^{N} \Gamma^j v_g g(n_3^j, n_2^j) = N\Gamma v_g g(n_3, n_2) = \frac{1}{\tau_p}. \tag{19}$$

For perfectly parabolic subbands, the expression for the gain may be approximated as

$$g(n_3, n_2) = a(n_3 - n_2), \tag{20}$$

where a is the differential gain. In the parabolic band approximation a is[23]

$$a = \frac{1}{L_p} \frac{4\pi q^2 z_{32}^2}{\epsilon_o n_{eff} \lambda_o (2\gamma_{32})}, \tag{21}$$

where z_{32} is the optical dipole matrix element, ϵ_o is the vacuum dielectric constant, n_{eff} is the effective index of the optical mode, λ_o is the lasing wavelength, $(2\gamma_{32})$ is the full width at half maximum (FWHM) of the optical transition, and L_p is the length of a single gain stage over which the integration is performed when calculating the mode-confinement factor Γ. The carrier and photon densities above threshold can be obtained by solving the equations

$$R_{31}(n_3, n_1) + R_{21}(n_2, n_1) \cong \frac{n_3}{\tau_{31}} + \frac{n_2}{\tau_{21}} = \frac{J}{q}, \tag{22}$$

$$\frac{J_{out}}{q} \cong \frac{n_1}{\tau_{out}} = \frac{J}{q}, \tag{23}$$

$$N\Gamma v_g a(n_3 - n_2) = \frac{1}{\tau_p}, \tag{24}$$

which results in

$$n_3 = \frac{J}{q} \frac{\tau_{21}\tau_{31}}{\tau_{21}+\tau_{31}} + \left(\frac{1}{N\Gamma v_g a \tau_p}\right) \frac{\tau_{31}}{\tau_{21}+\tau_{31}}, \tag{25}$$

$$n_2 = \frac{J}{q} \frac{\tau_{21}\tau_{31}}{\tau_{21}+\tau_{31}} - \left(\frac{1}{N\Gamma v_g a \tau_p}\right) \frac{\tau_{21}}{\tau_{21}+\tau_{31}}, \tag{26}$$

$$n_1 = \frac{J}{q} \tau_{out}, \tag{27}$$

$$S_p = \eta_r N \frac{(J - J_{th})}{q} \tau_p, \tag{28}$$

$$P_{out} = \eta_o \eta_r \frac{h\nu}{q} N(I - I_{th}), \tag{29}$$

where the threshold current density J_{th} and the radiative efficiency η_r are

$$J_{th} = \frac{q}{N\Gamma v_g a \tau_p} \left(\frac{1}{\tau_{32}} + \frac{1}{\tau_{31}}\right) \frac{1}{(1 - \tau_{21}/\tau_{32})}, \tag{30}$$

$$\eta_r = \left(1 - \frac{\tau_{21}}{\tau_{32}}\right) \frac{\tau_{31}}{(\tau_{21}+\tau_{31})}. \tag{31}$$

The radiative efficiency η_r for a QCL is defined as that fraction of the total number of electrons injected into each gain stage per second that contribute to photon emission.

Equations (25) and (26) show that above threshold, even though the gain is clamped to its threshold value, the electron densities keep increasing with the bias current. This is in contrast to what happens in a semiconductor diode laser in which the carrier density in the lasing state does not increase beyond its threshold value. As a result, an increase in the injected current density in QCL's does not only lead to an increase in the photon emission rate but it also leads to an increase in the rate of nonradiative transitions. For this reason, QCL's tend to have radiative efficiencies η_r significantly smaller than unity. If the lifetime τ_{21} of the electrons in the lower lasing state is much smaller than both the nonradiative lifetimes, τ_{32} and τ_{31}, then the electron densities in levels 3 and 2 would not increase much beyond threshold, and the radiative efficiency η_r would be close to unity. As will be shown later, the value of η_r has a significant impact on the noise properties of QCL's.

Figure 4 shows the electron densities n_3 and n_2 plotted as a function of the bias current. The values of the various device parameters used in generating Fig. 4 belong to the QCL reported in Ref. 11, and these values are given in Table I. Figure 4 shows that the rate of change of electron densities in levels 3 and 2 with the bias current exhibits discontinuities at threshold. This can be confirmed by comparing Eqs. (25) and (26) with Eqs. (16) and (17). As will be shown later in this paper, these discontinuities in the rate of increase of electron densities with the bias current result in a discontinuity in the value of the differential resistance of the laser at threshold.

V. THEORETICAL MODEL FOR NOISE AND FLUCTUATIONS

The model for the noise presented in this paper consists of a set of coupled self-consistent Langevin rate equations for the fluctuations in the electron density in different energy levels of a gain stage. Fluctuations in the electron density are caused by radiative and nonradiative scattering processes, electron-tunneling processes, and also by fluctuations in the current injected into the gain stage. Fluctuations in the current are a relaxational response to electron-scattering and
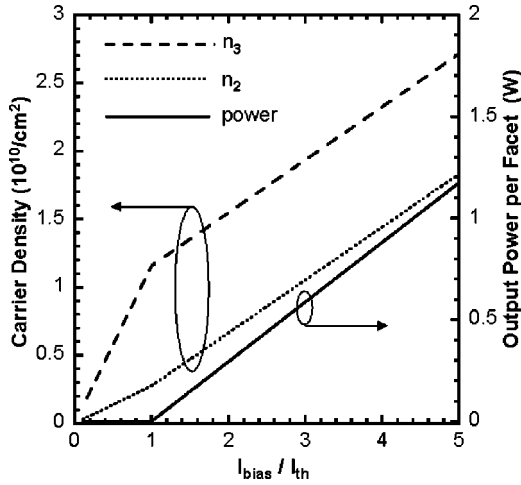
FIG. 4. Electron densities in level 3 and level 2 of the gain stage and the output power per facet are plotted as a function of the bias current. There is a discontinuity in the rate of increase of the electron densities with the bias current at threshold. For values of the QCL parameters see Table I.

tunneling events occurring inside all the gain stages of the QCL, and they are also caused by sources external to the laser that include thermal noise sources associated with circuit resistances. Photon-density fluctuations are also modeled by Langevin rate equations. Electron-density fluctuations in different gain stages are all coupled to the photon-density fluctuations and also to the fluctuations in the current that flows through all the gain stages connected in series. The system of equations obtained this way can easily be solved analytically or numerically to give the spectral density of the photon-number fluctuations and the current fluctuations. The methods described in this paper can be used to study a variety of QCL's that have been reported in the literature.

A. Linearized Langevin rate equations for electron and photon densities

The nonlinear rate equations can be linearized around any bias point to obtain rate equations for the fluctuations. Linearized Langevin rate equations for these fluctuations are

$$\frac{d\,\delta n_3^j}{dt} = \frac{\delta J_{in}^j}{q} - \frac{\delta n_3^j}{\tau_{32}} - \frac{\delta n_3^j}{\tau_{31}} - \Gamma^j v_g \left[a(\delta n_3^j - \delta n_2^j)\left(S_p + \frac{n_{sp}}{WL}\right) \right.$$
$$\left. + g(n_3^j, n_2^j)\delta S_p \right] - f_{32}^j - f_{31}^j - f_{RN}^j, \tag{32}$$

$$\frac{d\,\delta n_2^j}{dt} = \frac{\delta n_3^j}{\tau_{32}} - \frac{\delta n_2^j}{\tau_{21}} + \Gamma^j v_g \left[a(\delta n_3^j - \delta n_2^j)\left(S_p + \frac{n_{sp}}{WL}\right) \right.$$
$$\left. + g(n_3^j, n_2^j)\delta S_p \right] + f_{32}^j - f_{21}^j + f_{RN}^j, \tag{33}$$

$$\frac{d\,\delta n_1^j}{dt} = \frac{\delta n_3^j}{\tau_{31}} + \frac{\delta n_2^j}{\tau_{21}} + f_{31}^j + f_{21}^j - \frac{\delta J_{out}^j}{q}, \tag{34}$$

$$\frac{d\,\delta S_p}{dt} = \sum_{j=1}^N \Gamma^j v_g \left[a(\delta n_3^j - \delta n_2^j)\left(S_p + \frac{n_{sp}}{WL}\right) + g(n_3^j, n_2^j)\delta S_p \right]$$
$$- \frac{\delta S_p}{\tau_p} - F_L + \sum_{j=1}^N f_{RS}^j, \tag{35}$$

$$\delta P_{out} = \eta_o h\nu \frac{WL\delta S_p}{\tau_p} + F_o. \tag{36}$$

Equations (11)–(13) have been used above for approximating the transition rates R_{qk}. f_{32}, f_{31}, and f_{21} are Langevin sources that model the noise associated with the nonradiative intersubband transitions and also the radiative transitions into the nonlasing modes. f_{RN} and f_{RS} are Langevin sources that model the noise in photon emission and absorption from the lasing mode. F_L and F_o describe the noise associated with photon loss from the cavity.[21] All the Langevin noise sources have a white spectral density and their correlations can be found by the methods described in Ref. 21. All the nonzero correlations among the noise sources are given in Appendix A.

B. Linearized electron transport, Coulomb correlations and noise

In order to determine δJ_{in}^j and J_{out}^j the electron transport through the active region needs to be looked at in detail. Self-consistent modeling of electron transport in multiple quantum-well structures poses a significant challenge and the steady-state current-voltage characteristics of QCL's are difficult to compute accurately. In this paper a slightly different approach has been adopted that is more useful for the problem under consideration. A self-consistent model for the fluctuations in the electron-current density and the electron-charge density is presented. It is shown that self-consistent analysis of current density and charge-density fluctuations can be carried out in terms of only a few device parameters. The values of these parameters can either be determined experimentally or computed theoretically from more detailed self-consistent transport models. The method used in this paper to estimate the value of each parameter will be discussed when we compare the theoretical model with the experimental results.

The expression for the direct sequential tunneling current density from the injector state into level 3 of the gain stage can be written as[24]

$$J_{in} = J_{in-forward} - J_{in-backward}$$
$$= 2q \int \frac{d^2\vec{k}}{(2\pi)^2} \int \frac{d^2\vec{k}'}{(2\pi)^2} \frac{2\pi}{\hbar} |T_{\vec{k},\vec{k}'}|^2$$
$$\times \int_{-\infty}^{\infty} dE A[E - E_{inj}(\vec{k})]A[E - E_3(\vec{k}')]$$
$$\times [f(E - \mu_{inj}) - f(E - \mu_3)], \tag{37}$$

where the forward and backward components of the injection current are

TABLE I. Device parameters used in numerical simulations (From Ref. 11).

Parameter	Value
Lasing wavelength λ	5.0 μm
Operating temperature	20 K
Number of gain stages N	25 (unless stated otherwise)
Total confinement factor $\Sigma_{j=1}^{N}\Gamma^j$	$\mathrm{erf}(0.019\,N) \approx 0.02\,N$
Cavity width W	11.7 μm
Cavity length L	3 mm
Facet reflectivities r_1, r_2	0.27
Cavity internal loss α_i	11 cm^{-1}
Mode-effective index n_{eff}	3.29
Mode-group index n_g	3.4
Differential gain a	$\sim 4.0 \times 10^{-9}$ cm
Length of a single gain stage L_p	45.3 nm
$\tau_{in}, \tau_{out}, \tau_3$	1.0 ps
τ_2, τ_1	∞
τ_{32}	2.1 ps
τ_{31}	3.4 ps
τ_{21}	0.5 ps
C_{inj}	0.31 μF/cm^2
C_3, C_2	0.56 μF/cm^2
C_1	0.81 μF/cm^2
χ_{in}, χ_{out}	~ 1

$$J_{in-forward} = 2q \int \frac{d^2\vec{k}}{(2\pi)^2} \int \frac{d^2\vec{k}'}{(2\pi)^2} \frac{2\pi}{\hbar} |T_{\vec{k},\vec{k}'}|^2$$

$$\times \int_{-\infty}^{\infty} dE\, A[E - E_{inj}(\vec{k})]A[E - E_3(\vec{k}')]$$

$$\times f(E - \mu_{inj})[1 - f(E - \mu_3)], \qquad (38)$$

$$J_{in-backward} = 2q \int \frac{d^2\vec{k}}{(2\pi)^2} \int \frac{d^2\vec{k}'}{(2\pi)^2} \frac{2\pi}{\hbar} |T_{\vec{k},\vec{k}'}|^2$$

$$\times \int_{-\infty}^{\infty} dE\, A[E - E_{inj}(\vec{k})]A[E - E_3(\vec{k}')]$$

$$\times f(E - \mu_3)[1 - f(E - \mu_{inj})], \qquad (39)$$

where $T_{\vec{k},\vec{k}'}$ is the coupling constant and is related to the transmission probability. $E_{inj}(\vec{k})$ and $E_3(\vec{k})$ are the energies of electrons in the injector state and level 3 of the gain stage, respectively. $A(E)$ is a normalized Lorentzian function with FWHM equal to the broadening of the energy levels, and $f(E - \mu)$ is the Fermi-Dirac distribution function with a chemical potential μ. Expressions similar to Eq. (37) can also be written for the phonon assisted tunneling current density. The analysis presented in this paper is independent of the specific nature of the electron-tunneling mechanisms. In what follows, E_{inj} and E_3 will stand for $E_{inj}(\vec{k}=0)$ and $E_3(\vec{k}=0)$, respectively. The tunneling current in Eq. (37) depends upon the following three quantities: the difference $(\mu_{inj} - E_{inj})$ between the injector chemical potential and the energy of the injector state; the difference $(\mu_3 - E_3)$ between the chemical potential and the energy of level 3 of the gain stage; the relative difference $(E_{inj} - E_3)$ between the energies of the injector state and level 3 of the gain stage. The current can change if the number of electrons in the injector level or in level 3 of the gain stage changes. The current can also change if the energy of the injector level shifts with respect to the energy of level 3. δJ_{in} can be written as

$$\delta J_{in}^j = \frac{\delta J_{in}/\delta(\mu_{inj}-E_{inj})}{\delta n_{inj}/\delta(\mu_{inj}-E_{inj})}\delta n_{inj}^j + \frac{\delta J_{in}/\delta(\mu_3-E_3)}{\delta n_3/\delta(\mu_3-E_3)}\delta n_3^j$$

$$+ \frac{\delta J_{inj}}{\delta(E_{inj}-E_3)}(\delta E_{inj}^j - \delta E_3^j) + qf_{in}^j \quad (40)$$

$$= \frac{\delta J_{in}}{\delta n_{inj}}\delta n_{inj}^j + \frac{\delta J_{in}}{\delta n_3}\delta n_3^j + \frac{\delta J_{inj}}{\delta(E_{inj}-E_3)}$$

$$\times(\delta E_{inj}^j - \delta E_3^j) + qf_{in}^j, \quad (41)$$

where f_{in} is a Langevin noise source that models the noise in electron tunneling. Noise in electron transport by sequential tunneling in multiple quantum-well structures can be described with Langevin noise sources. In Refs. 2,3 the current noise in double-barrier resonant-tunneling structures is evaluated using classical discrete master equations. Under suitable conditions a discrete master equation may be converted into a Fokker-Planck equation, and if the fluctuations are relatively small a Fokker-Planck equation can be linearized around a stable steady-state solution (see Ref. 25 for details). Langevin rate equations can be used in place of linearized Fokker-Planck equations since the two formalisms are equivalent.[25] It can be shown that Langevin rate equations yield results identical to those presented in Refs. 2,3 for the current noise in double-barrier resonant-tunneling devices.[26] A linearized analysis based on Langevin rate equations may become invalid for highly nonlinear devices. The correlation function for the noise source f_{in} is

$$WL\langle f_{in}^j(t)f_{in}^q(t')\rangle = \frac{1}{q}(J_{in-forward}+J_{in-backward})$$

$$\times \delta_{jq}\delta(t-t') \quad (42)$$

$$\approx \frac{J_{in}}{q}\chi_{in}\delta_{jq}\delta(t-t'). \quad (43)$$

The factor χ_{in} relates the sum of the forward and backward tunneling currents to their difference which is the total injection current J_{in}. At low temperatures χ_{in} is expected to be close to unity since Pauli's exclusion would restrict the available phase space for the backward tunneling current.[3] For the same reason χ_{in} is expected to be close to unity for large values of the injection current J_{in}. At high temperatures and small values of the injection current, χ_{in} can be larger than unity.

Although Eq. (41) for the change in current density is derived for the case of direct sequential tunneling, it also holds for the case of phonon assisted tunneling. Even if the energy distribution of electrons inside each energy level in the steady state were not a Fermi-Dirac distribution with a well-defined chemical potential, Eq. (41) would still hold.

It is assumed that the superlattice injector is doped in regions not close to the gain stage. Electric-field lines from electron-density fluctuations δn_{inj}^j, δn_3^j, δn_2^j, and δn_1^j are imaged on the ionized dopants in the injector layer of the
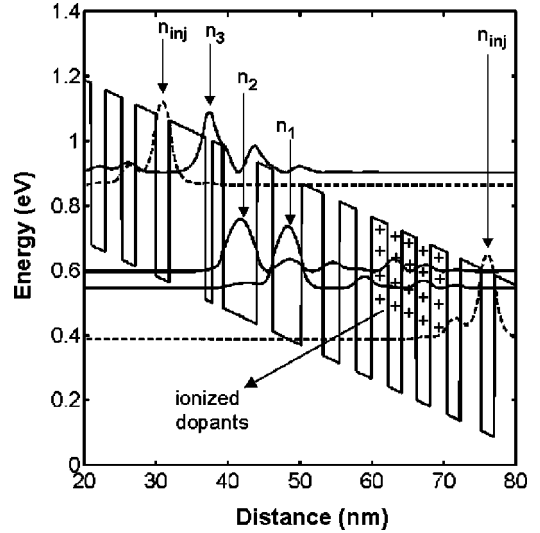

FIG. 5. Charge densities associated with the electron densities δn_{inj}, δn_3, δn_2, and δn_1 are shown. The electron charge densities are imaged on the positively charged ionized dopants present in the superlattice injector of the subsequent stage.

$(j+1)$th gain stage, as shown in Fig. 5. Therefore, the fluctuation δV^j in the potential difference across the jth gain stage can be written as

$$\delta V^j = \frac{q\,\delta n_{inj}^j}{C_{inj}} + \frac{q\,\delta n_3^j}{C_3} + \frac{q\,\delta n_2^j}{C_2} + \frac{q\,\delta n_1^j}{C_1}, \quad (44)$$

where C_{inj}, C_3, C_2, and C_1 are capacitances that relate the incremental change in the potential difference across a gain stage to the changes in the electron densities in different energy levels. Using first-order quantum-mechanical perturbation theory, $\delta E_{inj}^j - \delta E_3^j$ can be related to the fluctuation in the average potential difference between the injector level and level 3 of the gain stage. The fluctuation in the average potential difference between these two levels can also be expressed in terms of capacitances. The expression for $\delta E_{inj}^j - \delta E_3^j$, therefore, becomes

$$\delta E_{inj}^j - \delta E_3^j = \frac{q^2\,\delta n_{inj}^j}{C'_{inj}} - \frac{q^2\,\delta n_3^j}{C'_3} - \frac{q^2\,\delta n_2^j}{C'_2} - \frac{q^2\,\delta n_1^j}{C'_1}. \quad (45)$$

Using Eqs. (44) and (45), Eq. (41) can be cast in the form,

$$\frac{\delta J_{in}^j}{q} = \left(\frac{1}{t_{in}}+\frac{G_{in}}{C'_{inj}}\right)\delta n_{inj}^j - \left(\frac{1}{t_3}+\frac{G_{in}}{C'_3}\right)\delta n_3^j$$

$$-\left(\frac{G_{in}}{C'_2}\right)\delta n_2^j - \left(\frac{G_{in}}{C'_1}\right)\delta n_1^j + f_{in}^j \quad (46)$$

$$= \left(\frac{C_{inj}}{t_{in}} + \frac{C_{inj}}{C'_{inj}} G_{in} \right) \frac{\delta V^j}{q} - \left[\left(\frac{1}{t_{in}} + \frac{G_{in}}{C'_{inj}} \right) \frac{C_{inj}}{C_3} \right.$$

$$+ \left(\frac{1}{t_3} + \frac{G_{in}}{C'_3} \right) \right] \delta n_3^j - \left[\left(\frac{1}{t_{in}} + \frac{G_{in}}{C'_{inj}} \right) \frac{C_{inj}}{C_2} + \left(\frac{G_{in}}{C'_2} \right) \right] \delta n_2^j$$

$$- \left[\left(\frac{1}{t_{in}} + \frac{G_{in}}{C'_{inj}} \right) \frac{C_{inj}}{C_1} + \left(\frac{G_{in}}{C'_1} \right) \right] \delta n_1^j + f_{in}^j . \quad (47)$$

In Eq. (47) G_{in}, t_{in}, and t_3 are given by

$$G_{in} = q \frac{\delta J_{in}}{\delta (E_{inj} - E_3)}, \quad \frac{1}{t_{in}} = \frac{1}{q} \frac{\delta J_{in}}{\delta n_{inj}}, \quad \frac{1}{t_3} = - \frac{1}{q} \frac{\delta J_{in}}{\delta n_3} . \quad (48)$$

More generally, there may be more than just one energy level in the injector from which electrons get injected into level 3 of the gain stage. Equation (46) can be modified appropriately to take into account the contributions from all the energy levels inside the injector. However, if the values of t_{in} are roughly the same for all such states in the injector then the final form of Eq. (46) will remain unchanged, but δn_{inj} will then represent the total electron density in all the injector states.

Similarly, the fluctuation δJ_{out}^j in the tunneling current density from level 1 of the gain stage into the injector is given by the expression

$$\delta J_{out}^j = \frac{\delta J_{out} / \delta (\mu_1 - E_1)}{\delta n_1 / \delta (\mu_1 - E_1)} \delta n_1^j + \frac{\delta J_{out}}{\delta (E_1 - E'_{inj})}$$

$$\times (\delta E_1^j - \delta E_{inj}^{'j}) + q f_{out}^j \quad (49)$$

$$= \frac{\delta J_{out}}{\delta n_1} \delta n_1^j + \frac{\delta J_{out}}{\delta (E_1 - E'_{inj})} (\delta E_1^j - \delta E_{inj}^{'j}) + q f_{out}^j . \quad (50)$$

The Langevin noise source f_{out}^j has the correlation function

$$WL \langle f_{out}^j(t) f_{out}^q(t') \rangle = \frac{1}{q} (J_{out-forward}$$

$$+ J_{out-backward}) \delta_{jq} \delta(t - t') \quad (51)$$

$$\approx \frac{J_{out}}{q} \chi_{out} \delta_{jq} \delta(t - t') . \quad (52)$$

In a well-designed QCL the backward tunneling current from the injector of the next stage into level 1 of the gain stage is small and χ_{out} is expected to be close to unity. $E_{inj}^{'j}$ is the energy of the injector level of the next stage into which electrons tunnel from level 1 of the gain stage. $\delta E_1^j - \delta E_{inj}^{'j}$, as before, can be expressed in terms of capacitances

$$\delta E_1^j - \delta E_{inj}^{'j} = \frac{q^2 \delta n_{inj}^j}{C''_{inj}} + \frac{q^2 \delta n_3^j}{C''_3} + \frac{q^2 \delta n_2^j}{C''_2} + \frac{q^2 \delta n_1^j}{C''_1} . \quad (53)$$

Using Eqs. (44) and (53), δJ_{out}^j becomes

$$\frac{\delta J_{out}^j}{q} = \left(\frac{C_{inj}}{C''_{inj}} G_{out} \right) \frac{\delta V^j}{q} - \left(\frac{G_{out}}{C''_{inj}} \frac{C_{inj}}{C_3} - \frac{G_{out}}{C''_3} \right) \delta n_3^j$$

$$- \left(\frac{G_{out}}{C''_{inj}} \frac{C_{inj}}{C_2} - \frac{G_{out}}{C''_2} \right) \delta n_2^j - \left[\frac{G_{out}}{C''_{inj}} \frac{C_{inj}}{C_1} \right.$$

$$- \left(\frac{1}{t_{out}} + \frac{G_{out}}{C''_3} \right) \right] \delta n_1^j + f_{out}^j , \quad (54)$$

where t_{out} and G_{out} are

$$\frac{1}{t_{out}} = \frac{1}{q} \frac{\delta J_{out}}{\delta n_1}; \quad G_{out} = q \frac{\delta J_{out}}{\delta (E_1 - E'_{inj})} . \quad (55)$$

In Eq. (49) it has been assumed that electrons in the injector relax into the ground state of the injector sufficiently fast so that electron occupation in the injector levels do not effect the electron escape rate out of level 1 of the gain stage.

Note that G_{in} and G_{out} can be positive or negative depending upon the relative alignment of the energy levels E_{inj} and E_3 in the steady state. The scheme used in deriving Eqs. (47) and (54) is fairly general and can be used to derive self-consistent linearized transport equations for a variety of QCL structures. Approximations can be made to simplify Eqs. (47) and (54). Expression for δJ_{in}^j can also be written as

$$\frac{\delta J_{in}^j}{q} = \frac{1}{\tau_{in}} \delta n_{inj}^j - \frac{1}{\tau_3} \delta n_3^j - \frac{1}{\tau_2} \delta n_2^j - \frac{1}{\tau_1} \delta n_1^j + f_{in}^j \quad (56)$$

$$= \left(\frac{C_{inj}}{\tau_{in}} \right) \frac{\delta V^j}{q} - \left(\frac{1}{\tau_{in}} \frac{C_{inj}}{C_3} + \frac{1}{\tau_3} \right) \delta n_3^j - \left(\frac{1}{\tau_{in}} \frac{C_{inj}}{C_2} \right.$$

$$+ \frac{1}{\tau_2} \right) \delta n_2^j - \left(\frac{1}{\tau_{in}} \frac{C_{inj}}{C_1} + \frac{1}{\tau_1} \right) \delta n_1^j + f_{in}^j . \quad (57)$$

For the sake of economy of notation new parameters have been introduced in the above equation

$$\frac{1}{\tau_{in}} = \frac{1}{t_{in}} + \frac{G_{in}}{C'_{inj}}, \quad \frac{1}{\tau_3} = \frac{1}{t_3} + \frac{G_{in}}{C'_3}, \quad \frac{1}{\tau_2} = \frac{G_{in}}{C'_2}, \quad \frac{1}{\tau_1} = \frac{G_{in}}{C'_1} . \quad (58)$$

Simple electrostatic arguments can be used to show that τ_2 and τ_1 will be large and can be assumed to be infinite.

The injector is assumed to have a large number of closely spaced energy levels. J_{out} is, therefore, largely insensitive to the relative shifts in E_1 and E'_{inj}. This implies that terms containing G_{out} in the expression for δJ_{out}^j may be neglected and the simplified expression for δJ_{out}^j becomes

$$\frac{\delta J_{out}^j}{q} = \frac{1}{\tau_{out}} \delta n_1^j + f_{out}^j , \quad (59)$$

where τ_{out} is just t_{out}. Equations (57) and (59) show that in addition to the parameters given in the electron and photon density rate equations [Eqs. (32)–(35)], the only other pa-

rameters necessary for describing electron transport through the gain stage are C_{inj}, C_3, C_2, C_1, τ_{in}, τ_3, τ_2, and τ_1.

C. Displacement currents

The noise current δJ_{ext}, which flows in the external circuit, is not equal to δJ_{in}^j or δJ_{out}^j. δJ_{ext} also includes displacement currents and is given by the expression

$$\delta J_{ext} = \delta J_{in}^j + q \frac{d\,\delta n_{inj}^j}{d\,t}. \tag{60}$$

Since all the gain stages are connected electrically in series, the same current δJ_{ext} flows through all the gain stages. The second term on the right-hand side of Eq. (60) is the contribution to δJ_{ext} from displacement currents. Differentiating both sides of Eq. (44) with respect to time and rearranging yields

$$q\frac{d\,n_{inj}^j}{d\,t} = C_{inj}\frac{d\,\delta V^j}{d\,t} - \sum_{k=1}^{3} q\frac{C_{inj}}{C_k}\frac{d\,\delta n_k^j}{d\,t}.$$

Using the above equation the expression for δJ_{ext} becomes

$$\delta J_{ext} = \delta J_{in}^j + C_{inj}\frac{d\,\delta V^j}{d\,t} - \sum_{k=1}^{3} q\frac{C_{inj}}{C_k}\frac{d\,\delta n_k^j}{d\,t} \tag{61}$$

$$= \delta J_{out}^j + C_{inj}\frac{d\,\delta V^j}{d\,t} + \sum_{k=1}^{3} q\left(1 - \frac{C_{inj}}{C_k}\right)\frac{d\,\delta n_k^j}{dt}. \tag{62}$$

Equation (62) follows from Eq. (61) by using the particle-number conservation equation

$$\sum_{k=1}^{3} q\frac{d\,\delta n_k^j}{dt} = \delta J_{in}^j - \delta J_{out}^j.$$

Equations (61) and (62) satisfy the Ramo-Shockley theorem.[27]

D. Differential resistance

Below threshold, the total differential resistance R_d of all the gain stages can be calculated by substituting Eqs. (16)–(18) in Eq. (57),

$$R_d = \frac{N}{WL}\frac{\tau_{in}}{C_{inj}}\left[1 + \left(\frac{1}{\tau_{in}}\frac{C_{inj}}{C_3} + \frac{1}{\tau_3}\right)\frac{\tau_{32}\tau_{31}}{\tau_{32}+\tau_{31}}\right.$$
$$\left. + \left(\frac{1}{\tau_{in}}\frac{C_{inj}}{C_2} + \frac{1}{\tau_2}\right)\frac{\tau_{21}\tau_{31}}{\tau_{32}+\tau_{31}} + \left(\frac{1}{\tau_{in}}\frac{C_{inj}}{C_1} + \frac{1}{\tau_1}\right)\tau_{out}\right] \tag{63}$$

$$= \frac{N}{WL}\frac{\tau_{in}}{C_{inj}}(1 + \theta_3' + \theta_2' + \theta_1). \tag{64}$$

Above threshold, the differential resistance can be computed by using Eqs. (25)–(27) with Eq. (57)

$$R_d = \frac{N}{WL}\frac{\tau_{in}}{C_{inj}}\left[1 + \left(\frac{1}{\tau_{in}}\frac{C_{inj}}{C_3} + \frac{1}{\tau_3}\right)\frac{\tau_{21}\tau_{31}}{\tau_{21}+\tau_{31}}\right.$$
$$\left. + \left(\frac{1}{\tau_{in}}\frac{C_{inj}}{C_2} + \frac{1}{\tau_2}\right)\frac{\tau_{21}\tau_{31}}{\tau_{21}+\tau_{31}} + \left(\frac{1}{\tau_{in}}\frac{C_{inj}}{C_1} + \frac{1}{\tau_1}\right)\tau_{out}\right] \tag{65}$$

$$= \frac{N}{WL}\frac{\tau_{in}}{C_{inj}}(1 + \theta_3 + \theta_2 + \theta_1). \tag{66}$$

Expressions for the parameters θ_3, θ_3', θ_2, θ_2', and θ_1 are given in Appendix B. Notice the similarity between Eqs. (64) and (66), and Eq. (F25) for the differential resistance of interband semiconductor diode lasers given in Appendix F. Unlike the active regions of diode lasers, the active regions of unipolar QCL's are not charge neutral and as a result various capacitances appear in the expression for the differential resistance of QCL's.

The discontinuity ΔR_d in the differential resistance at threshold for an N stage QCL is

$$\Delta R_d = \frac{N}{WL}\frac{\tau_{in}}{C_{inj}}\left[\left(\frac{1}{\tau_{in}}\frac{C_{inj}}{C_3} + \frac{1}{\tau_3}\right)\left(\frac{\tau_{32}\tau_{31}}{\tau_{32}+\tau_{31}} - \frac{\tau_{21}\tau_{31}}{\tau_{21}+\tau_{31}}\right)\right.$$
$$\left. + \left(\frac{1}{\tau_{in}}\frac{C_{inj}}{C_2} + \frac{1}{\tau_2}\right)\left(\frac{\tau_{21}\tau_{31}}{\tau_{32}+\tau_{31}} - \frac{\tau_{21}\tau_{31}}{\tau_{21}+\tau_{31}}\right)\right] \tag{67}$$

$$= \frac{N}{WL}\frac{\tau_{in}}{C_{inj}}[(\theta_3' - \theta_3) + (\theta_2' - \theta_2)]. \tag{68}$$

The incremental change in the potential drop across a gain stage is related to the incremental changes in electron densities through Eq. (44). Therefore, the discontinuity in the differential resistance at threshold results from the discontinuity at threshold in the rate of change of electron densities in levels 3 and 2 of the gain stage with the bias current. Figure 6 shows the calculated and measured differential resistance of a QCL as a function of the bias current. The experimental data is taken from Ref. 11. The values of the various device parameters are given in Table I. Values of τ_{21}, τ_{31}, and τ_{32} are taken from Ref. 11. Values of all the capacitances given in Table I are estimated from the structure of the QCL described in Ref. 11. Values of τ_{in}, τ_3, and τ_{out} are estimated from Eqs. (48) and (55). The total resistance of the ohmic contacts and the superlattice injectors is assumed to be approximately 0.3 Ω at threshold. The experimentally observed discontinuity in the differential resistance at threshold is exactly reproduced in the calculated results without the use of any fitting parameters. This agreement suggests that the self-consistent model for the linearized electron transport presented in this paper adequately captures the essential ingredients.

Diode lasers also exhibit a discontinuity in the differential resistance at threshold. As shown in Appendix F, the discontinuity in the differential resistance of diode lasers at threshold is $K_B T/qI_{th}$ times a factor of the order of unity, which can be compared with the more complicated expression given in Eq. (67) for QCL's.
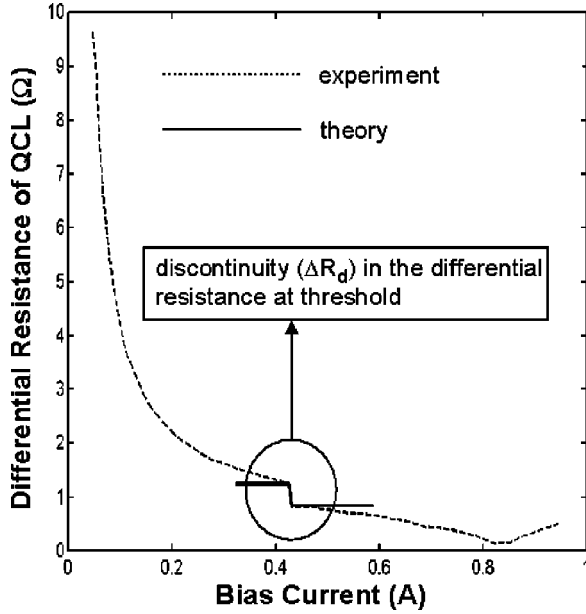
FIG. 6. Differential resistance of a QCL is shown as a function of the bias current. The experimentally measured discontinuity in the differential resistance at threshold is about 0.3 Ω. The theoretical model reproduces the discontinuity exactly. The experimental data is taken from Ref. 11.

E. Electron transport in the superlattice injector

In this paper no attention has been given to modeling the electron transport through the superlattice injector. In the absence of any bias current, the energy levels in the injector are not suitably aligned to facilitate electron transport and the resistance of the injector region is large. As the bias current is gradually increased electrons pile up in different quantum wells until their presence modifies the potential profile and aligns the energy levels such that the electron current can flow. Once the injector has been *turned on* in this fashion, the differential resistance of the injector region is negligible, and the only bottleneck for electron transport is the gain stage. As a result of the small differential resistance of the injector region, any current noise originating in the injector region will not couple well into the external circuit. Therefore, electron transport in the injector region may be ignored when modeling noise. If necessary, the impedance of the superlattice injectors can be modeled with a lumped element and the current noise generated inside the injector regions can be modeled with a voltage source in series (or a current source in parallel) with that element, as shown below. A detailed discussion of the current noise in superlattice structures is beyond the scope of this paper.

F. Biasing electrical circuit

Two electrical circuits for biasing QCL's are shown in Fig. 7. In circuit A, the QCL with an impedance $Z(\omega)$ is biased with a voltage source V_s in series with an impedance $Z_s(\omega)$. The thermal noise originating in the impedance $Z_s(\omega)$ is modeled by adding a voltage noise source δV_s. The differential impedance of the superlattice injector and the
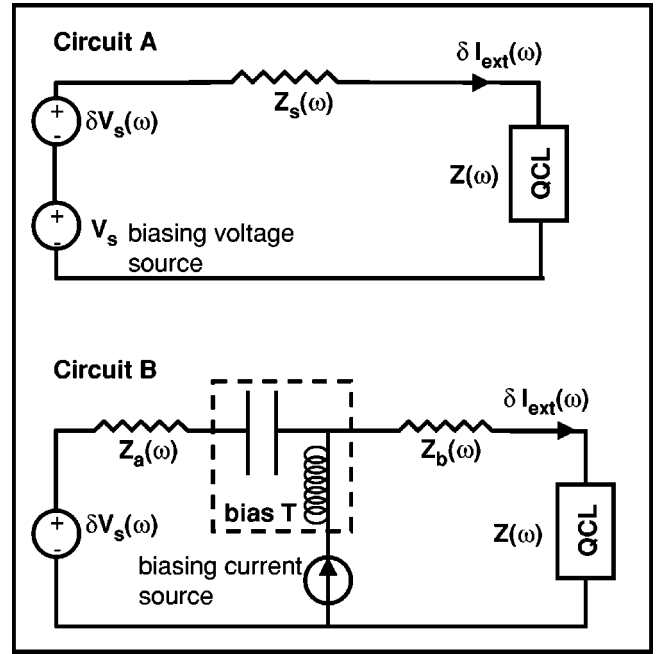

FIG. 7. Circuits used for biasing QCL's.

current noise generated by the injector can also be modeled with an impedance and a voltage noise source in series (or a current noise source in parallel) with that impedance. For the sake of economy of notation it will be assumed that the impedance $Z_s(\omega)$ represents not just an external circuit impedance but the Thevenin equivalent impedance of the superlattice injectors, device ohmic contacts, external circuit resistances, and device and circuit parasitics, and the voltage noise source δV_s represents the Thevenin equivalent of their individual noise sources. Only the gain stages inside the QCL are not included within $Z_s(\omega)$ and they are represented by the impedance $Z(\omega)$. However, $Z(\omega)$ will be loosely referred to as the impedance of the QCL. The current noise generated by the gain stages can also be modeled by adding a current noise source in parallel with $Z(\omega)$ as shown in later sections.

Direct-current modulation of the QCL can be achieved by adding an rf voltage source in series with V_s, and this rf voltage source can also be represented by the voltage source δV_s. From the context it will be clear whether δV_s represents a rf signal source or a noise source.

Semiconductor lasers are frequently biased as shown in circuit B in Fig. 7. The laser is biased with a current source in series with an ideal inductor, and it is also capacitively coupled to a voltage source δV_s with a series impedances $Z_a(\omega)$ and $Z_b(\omega)$. If at frequencies of interest the inductor and the coupling capacitor are almost open and short, respectively, then this circuit is also equivalent to circuit A. Therefore, in this paper only circuit A will be considered. In circuit A the current δI_{ext} can be expressed as

$$\delta I_{ext}(\omega) = \delta J_{ext}(\omega) WL = \frac{\delta V_s(\omega) - \sum_{j=1}^{N} \delta V^j(\omega)}{Z_s(\omega)}. \quad (69)$$
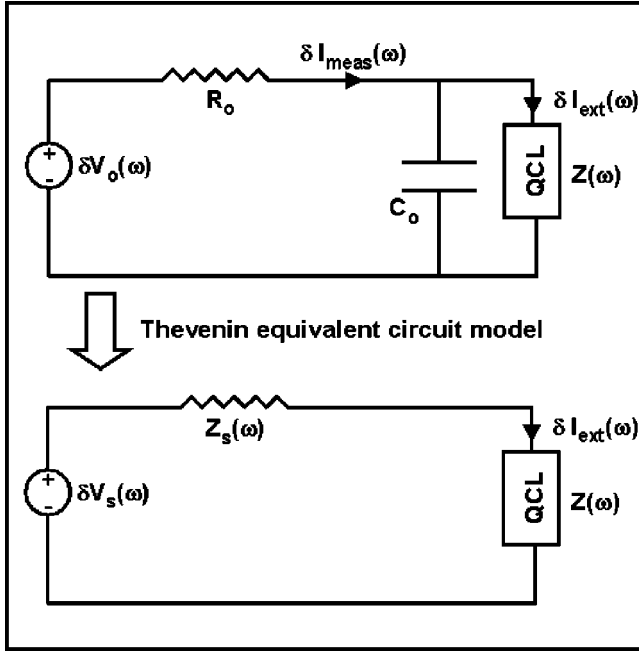
FIG. 8. Thevenin equivalent circuit model indicating the distinction between $\delta I_{ext}(\omega)$ and $\delta I_{meas}(\omega)$.

It is important to note here that $\delta I_{ext}(\omega)$ may not be the noise current that would be measured in an experiment. For example, suppose that the QCL has a parasitic capacitance C_o in parallel with the actual device, as shown in Fig. 8. The QCL is driven with a series resistor R_o and a noise voltage source $\delta V_o(\omega)$ representing the thermal noise in the resistor R_o. Figure 8 shows the distinction between the noise current $\delta I_{ext}(\omega)$ defined in Eq. (69) and the noise current $\delta I_{meas}(\omega)$ that would be measured in an experiment. Notice that the Thevenin equivalent impedance $Z_s(\omega)$ is a parallel combination of the resistance R_o and the capacitance C_o. $Z_s(\omega)$ and $\delta V_s(\omega)$ are

$$Z_s(\omega) = \frac{R_o}{(1 + j\omega R_o C_o)}, \quad \delta V_s(\omega) = \frac{\delta V_o(\omega)}{(1 + j\omega R_o C_o)},$$
(70)

and the relation between $\delta I_{ext}(\omega)$ and $\delta I_{meas}(\omega)$ is

$$\delta I_{ext}(\omega) = \frac{\delta I_{meas}(\omega)}{[1 + j\omega Z(\omega)C_o]}.$$
(71)

Choosing to define $Z_s(\omega)$ this way helps in formulating a noise model that is independent of the specific nature of the device parasitics.

VI. SOLUTION OF THE COUPLED EQUATIONS

A. Current modulation response

In this section, the response $\delta P_{out}(\omega)/\delta I_{ext}(\omega)$ of QCL's to external sinusoidal current modulation $\delta I_{ext}(\omega)$ is determined.[28] The frequency dependence of the photon-noise spectral density of semiconductor lasers is directly related to the frequency dependence of the current modulation response. It is, therefore, instructive to look at the modulation

response of QCL's. Some of the results discussed in this section were first presented by the authors in Ref. 26. The modulation response can be found by solving Eqs. (32)–(36), together with Eq. (57) and (59), and setting all the noise sources equal to zero. The external circuit constraints expressed in Eqs. (61) and (69) must also be enforced. Equations (32)–(34) for each gain stage are coupled to the same set of equations for all the other gain stages through Eqs. (35) and (61). Such a large system of coupled equations can be solved only numerically. A numerical approach, although simple to implement, is not very instructive. With the approximation that all gain stages have the same confinement factor Γ, a significant portion of the work can be done analytically. This approach will be followed in this paper. All equations, unless stated otherwise, will be expressed in the frequency domain.

The relationship between the current density $\delta J_{ext}(\omega)$, which flows in the external circuit and the total potential drop $\delta V(\omega)$ across all the gain section can be obtained by using Eq. (57) in Eq. (61), and summing over the index j

$$\frac{C_{inj}}{\tau_{in}} \frac{\delta V(\omega)}{q} = \frac{N}{(1 + j\omega\tau_{in})} \frac{\delta J_{ext}(\omega)}{q}$$

$$+ \sum_{k=1}^{3} \left[\frac{1}{\tau_{in}} \frac{C_{inj}}{C_k} + \frac{1}{\tau_k(1 + j\omega\tau_{in})} \right] \delta N_k(\omega).$$
(72)

The following new symbols have been introduced in Eq. (72),

$$\delta N_k(\omega) = \sum_{j=1}^{N} \delta n_k^j(\omega) \quad \text{where} \quad k = 1,2,3 \quad \text{and}$$

$$\delta V(\omega) = \sum_{j=1}^{N} \delta V^j(\omega).$$

Using Eqs. (57), (59), and (72) in Eqs. (32)–(35), summing over the index j and arranging the resulting equations in a matrix form gives

$$\begin{bmatrix} \mathbf{D}_{11} & \mathbf{D}_{12} & \mathbf{D}_{13} & 0 \\ 0 & \mathbf{D}_{22} & \mathbf{D}_{23} & \mathbf{D}_{24} \\ \mathbf{D}_{31} & \mathbf{D}_{32} & \mathbf{D}_{33} & \mathbf{D}_{34} \\ 0 & \mathbf{D}_{42} & \mathbf{D}_{43} & \mathbf{D}_{44} \end{bmatrix} \begin{bmatrix} \delta N_1(\omega) \\ \delta N_2(\omega) \\ \delta N_3(\omega) \\ \delta S_p(\omega) \end{bmatrix}$$

$$= \frac{N}{(1 + j\omega\tau_{in})} \frac{\delta J_{ext}(\omega)}{q} \begin{bmatrix} 0 \\ 0 \\ 1 \\ 0 \end{bmatrix}.$$
(73)

The coefficients of the matrix $\mathbf{D}$ can be found from Eqs. (32)–(35) and they are given in Appendix C. The solution of Eq. (73) can be written as

$$
\begin{bmatrix}
\delta N_1(\omega) \\
\delta N_2(\omega) \\
\delta N_3(\omega) \\
\delta S_p(\omega)
\end{bmatrix}
=
\begin{bmatrix}
\mathbf{D}_{13}^{-1}(\omega) \\
\mathbf{D}_{23}^{-1}(\omega) \\
\mathbf{D}_{33}^{-1}(\omega) \\
\mathbf{D}_{43}^{-1}(\omega)
\end{bmatrix}
\frac{N}{(1+j\omega\,\tau_{in})}\frac{\delta J_{ext}(\omega)}{q}.
\tag{74}
$$

The coefficients of the matrix $\mathbf{D}^{-1}$ are given in Appendix D. Equation (74) can be used in Eq. (72) to calculate the total impedance $Z(\omega)$ of all the gain stages

$$
Z(\omega) = \frac{N}{WL}\frac{\tau_{inj}}{C_{inj}}\frac{1}{(1+j\omega\,\tau_{in})}\left[1+\sum_{k=1}^{3}\left(\frac{1}{\tau_{in}}\frac{C_{inj}}{C_k}\right.\right.
$$
$$
\left.\left.+\frac{1}{\tau_k(1+j\omega\,\tau_{in})}\right)\mathbf{D}_{k3}^{-1}(\omega)\right],
\tag{75}
$$

$Z(\omega=0)$ is just the differential resistance R_d of the QCL given earlier in Eqs. (63) and (65). Finally, from Eqs. (36) and (74), the current modulation response can be written as

$$
\frac{\delta P_{out}(\omega)}{\delta I_{ext}(\omega)} = \eta_o\frac{h\nu}{q}\frac{N}{\tau_p}\frac{\mathbf{D}_{43}^{-1}(\omega)}{(1+j\omega\,\tau_{in})}.
\tag{76}
$$

In QCL's that have been reported in the literature the photon lifetime τ_p is usually much longer than any other relevant time constant of the laser. Therefore, it is expected that the bandwidth of the modulation response in QCL's will be limited by the inverse photon lifetime. Above threshold, an analytical approximation for the modulation response valid for values of ω smaller than $1/\tau_{in}, 1/\tau_{st}$, and $1/\tau_{21}$ can be found in the limit $\{\tau_2,\tau_1\}\rightarrow\infty$ (see Appendix D)

$$
\frac{\delta P_{out}(\omega)}{\delta I_{ext}(\omega)} = \eta_o\eta_r\frac{h\nu}{q}N\frac{\omega_R^2}{(\omega_R^2-\omega^2+j\omega\gamma)},
\tag{77}
$$

where η_r is the radiative efficiency defined in Eq. (31), and the relaxation oscillation frequency ω_R and the damping constant γ are

$$
\omega_R^2 = \frac{\dfrac{1}{\tau_p\,\tau_{st}}\left(1+\dfrac{\tau_{21}}{\tau_{31}}\right)}{\left[1+\dfrac{\tau_{21}}{\tau_{31}}+\dfrac{\tau_{21}}{\tau_{32}}+\dfrac{\tau_{in}}{\tau_3}+\dfrac{\tau_{21}}{\tau_{st}}\left(2+\dfrac{\tau_{in}}{\tau_3}\right)\right]},
\tag{78}
$$

$$
\gamma = \frac{\left[\dfrac{1}{\tau_{st}}\left(1+\dfrac{\tau_{21}}{\tau_{31}}\right)+\dfrac{1}{\tau_{31}}+\dfrac{1}{\tau_{32}}+\dfrac{\tau_{21}}{\tau_p\,\tau_{st}}\left(2+\dfrac{\tau_{in}}{\tau_3}\right)\right]}{\left[1+\dfrac{\tau_{21}}{\tau_{31}}+\dfrac{\tau_{21}}{\tau_{32}}+\dfrac{\tau_{in}}{\tau_3}+\dfrac{\tau_{21}}{\tau_{st}}\left(2+\dfrac{\tau_{in}}{\tau_3}\right)\right]}.
\tag{79}
$$

In the above expressions τ_{st} is the differential lifetime associated with stimulated and spontaneous photon emission into the lasing mode and is given by the relation

$$
\frac{1}{\tau_{st}} = \Gamma v_g a\left(S_p+\frac{n_{sp}}{WL}\right).
\tag{80}
$$

Equation (77) has the standard form used for semiconductor diode lasers (see Appendix F and Ref. 21). The damping constant γ can be related to ω_R

$$
\gamma = K\,\omega_R^2+\gamma_o,
\tag{81}
$$

where

$$
K = \tau_p,
\tag{82}
$$

$$
\gamma_o = \frac{\left[\dfrac{1}{\tau_{31}}+\dfrac{1}{\tau_{32}}+\dfrac{\tau_{21}}{\tau_p\,\tau_{st}}\left(2+\dfrac{\tau_{in}}{\tau_3}\right)\right]}{\left[1+\dfrac{\tau_{21}}{\tau_{31}}+\dfrac{\tau_{21}}{\tau_{32}}+\dfrac{\tau_{in}}{\tau_3}+\dfrac{\tau_{21}}{\tau_{st}}\left(2+\dfrac{\tau_{in}}{\tau_3}\right)\right]}.
\tag{83}
$$

The K factor describes the damping of the QCL modulation response at high photon densities. γ_o has a weak dependence on the photon density through τ_{st} and it approaches $1/\tau_p$ at large photon densities.

If the condition $\omega_R<\gamma/2$ is satisfied then Eq. (77) describes a second-order overdamped system. For QCL's that have been reported in the literature this condition holds true above threshold. Using the values of device parameters from Table I, ω_R and γ can be calculated. If we assume that the output power of the laser is around 150 mW, then from Eqs. (6) and (80) τ_p and τ_{st} are approximately 7 ps and 2.8 ps, respectively. The resulting value of γ is more than three times larger than that of ω_R. The internal time constants in QCL's are usually smaller than the photon lifetime τ_p and, therefore, the modulation response of QCL's is overdamped. An overdamped modulation response implies the absence of relaxation oscillations. In contrast, the current modulation response of semiconductor diode lasers is underdamped and becomes overdamped only at very large bias currents when τ_{st} becomes small.[21]

For QCL's, the 3-dB frequency, which is defined to be the frequency at which the square modulus of the laser modulation response becomes one-half of its value at zero frequency, can be found from the simplified expression for the modulation response in Eq. (77)

$$
\omega_{3dB}^2 = \sqrt{\left(\frac{\gamma^2}{2}-\omega_R^2\right)^2+\omega_R^4}-\left(\frac{\gamma^2}{2}-\omega_R^2\right).
\tag{84}
$$

As the photon density inside the laser cavity increases the 3-dB frequency also increases but it asymptotically approaches an upper limit $\omega_{3dB|max}$. This maximum attainable 3-dB bandwidth can be calculated from Eq. (84) and it comes out to be

$$
\omega_{3dB|max} \approx \frac{1}{\tau_p}.
\tag{85}
$$

Equation (85) confirms the intuition that a laser cannot be modulated much faster than the inverse of the photon lifetime inside the laser cavity. As long as the photon lifetime τ_p is much longer than τ_{in}, τ_{st}, and τ_{21} the approximations made in deriving Eq. (77) are justified. Otherwise the exact expression given in Eq. (76) must be evaluated numerically. As shown in Appendix F, in diode lasers the value of
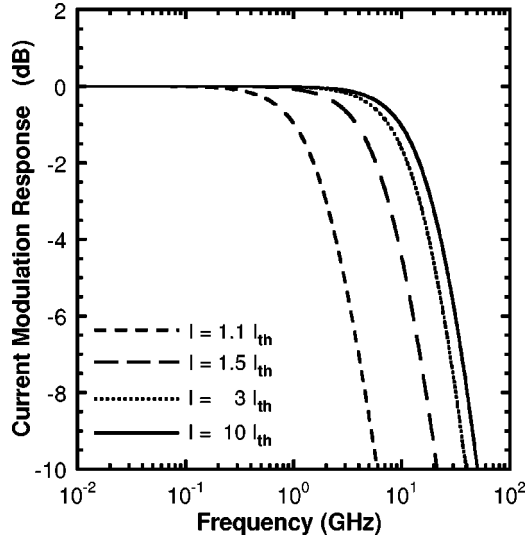
FIG. 9. Absolute value squared of the direct-current modulation response is plotted as a function of the frequency for different bias currents. Modulation response shown in the figure has been normalized with respect to its value at zero frequency. For values of the QCL parameters see Table I.

$\omega_{3dB|max}$ equals $\sqrt{2}/\tau_p$. The difference of a factor of $\sqrt{2}$ comes from the fact that in diode lasers the modulation response is underdamped (see Appendix F).

As in diode lasers, the photon lifetime imposes a fundamental limit on how fast QCL's can be modulated. It is not uncommon to find predictions of tetrahertz modulation bandwidths for QCL's in literature.[29] However, for all the QCL's reported in the literature so far, the photon lifetime is the longest of all the time constants and it is the dominant factor that would limit the modulation bandwidth of these QCL's to tens of gigahertz instead of tetrahertz. It remains to be seen if QCL structures can be designed in which the photon lifetime is not the bottleneck for the modulation bandwidth.

Figure 9 shows the calculated modulation response of a QCL as a function of the frequency for different values of the bias current. The values of the different parameters of the QCL are taken from Ref. 11 and are given in Table I. In the numerical calculations values of all the device time constants (except τ_{st}) were assumed to be independent of the bias. Figure 9 shows that at low bias currents the 3-dB frequency increases with the bias current and at high bias currents the 3-dB frequency saturates to a value that is well approximated by $1/(2\pi\tau_p)=21$ GHz. The analysis carried out in this paper does not take into account device heating that may also be important in limiting the modulation bandwidth of QCL's at large bias currents.

Figure 10 shows the impedance $Z(\omega)$ of the QCL plotted as a function of the frequency for different bias currents. The peaks in the values of $Z(\omega)$ are not due to relaxation oscillations since, as already pointed out earlier, the modulation response of the QCL is overdamped. The peaks are due to the fact that the smallest zero of $Z(\omega)$ is at a frequency that is smaller than the frequency of its smallest pole. Impedance measurements can, therefore, provide valuable information about the time scales associated with electron dynamics in QCL's.
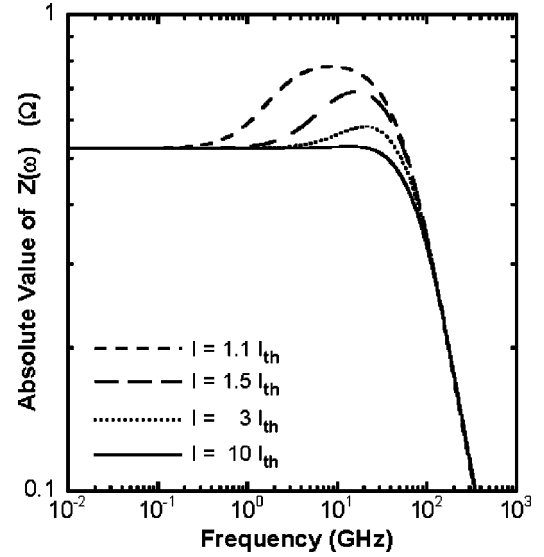

FIG. 10. Absolute value of the impedance $Z(\omega)$ is plotted as a function of the frequency for different bias currents. The peaks in the values of $Z(\omega)$ are not because of relaxation oscillations, since the modulation response of the QCL is overdamped, but because the smallest zero of $Z(\omega)$ is smaller than its smallest pole. For values of the QCL parameters see Table I.

B. Laser intensity noise and current noise

In this section the current noise in the external circuit and the intensity noise in the output power from QCL's is calculated. In the Langevin equation formalism noise is added through the Langevin noise sources that were introduced in Eqs. (32)–(36) and also in Eqs. (57) and (59). In addition, any noise originating in the external circuit and in the superlattice injectors can also contribute to the current noise and the photon noise and as already explained earlier, this noise can be represented by the voltage source δV_s. In this paper it is assumed that δV_s represents the thermal noise originating in the series impedance $Z_s(\omega)$ and its correlation function is

$$\langle \delta V_s(\omega) \delta V_s(\omega') \rangle = 2 K_B T \, \mathrm{Re}\{Z_s(\omega)\} 2\pi \, \delta(\omega - \omega').$$

(86)

By assuming the above correlation function for the noise source δV_s, we are ignoring any noise that may be contributed by the superlattice injectors.

Including the Langevin noise sources Eq. (73) can be written as

$$\begin{bmatrix} D_{11} & D_{12} & D_{13} & 0 \\ 0 & D_{22} & D_{23} & D_{24} \\ D_{31} & D_{32} & D_{33} & D_{34} \\ 0 & D_{42} & D_{43} & D_{44} \end{bmatrix} \begin{bmatrix} \delta N_1(\omega) \\ \delta N_2(\omega) \\ \delta N_3(\omega) \\ \delta S_p(\omega) \end{bmatrix}$$

$$= \frac{N}{(1+j\omega\tau_{in})} \frac{\delta J_{ext}(\omega)}{q} \begin{bmatrix} 0 \\ 0 \\ 1 \\ 0 \end{bmatrix} + \begin{bmatrix} F_1(\omega) \\ F_2(\omega) \\ F_3(\omega) \\ F_4(\omega) \end{bmatrix}.$$

(87)

The expressions for the noise sources F_1, F_2, F_3, and F_4 are

$$F_1(\omega) = \sum_{j=1}^{N} F_1^j = \sum_{j=1}^{N} [f_{31}^j(\omega) + f_{21}^j(\omega) - f_{out}^j(\omega)],$$

(88)

$$F_2(\omega) = \sum_{j=1}^{N} F_2^j = \sum_{j=1}^{N} [f_{32}^j(\omega) - f_{21}^j(\omega) + f_{RN}^j(\omega)],$$

(89)

$$F_3(\omega) = \sum_{j=1}^{N} F_3^j = \sum_{j=1}^{N} \left[f_{in}^j(\omega) \frac{j\omega\,\tau_{in}}{(1 + j\omega\,\tau_{in})} \right.$$
$$\left. - f_{32}^j(\omega) - f_{31}^j(\omega) - f_{RN}^j(\omega) \right],$$

(90)

$$F_4(\omega) = \sum_{j=1}^{N} F_4^j = \sum_{j=1}^{N} \left[f_{RS}^j(\omega) - \frac{F_L(\omega)}{N} \right].$$

(91)

The solution of Eq. (87) can be written as

$$\begin{bmatrix} \delta N_1(\omega) \\ \delta N_2(\omega) \\ \delta N_3(\omega) \\ \delta S_p(\omega) \end{bmatrix} = \begin{bmatrix} \mathbf{D}_{13}^{-1}(\omega) \\ \mathbf{D}_{23}^{-1}(\omega) \\ \mathbf{D}_{33}^{-1}(\omega) \\ \mathbf{D}_{43}^{-1}(\omega) \end{bmatrix} \frac{N}{(1 + j\omega\,\tau_{in})} \frac{\delta J_{ext}(\omega)}{q}$$

$$+ \begin{bmatrix} \sum_{l=1}^{4} \mathbf{D}_{1l}^{-1}(\omega) F_l(\omega) \\ \sum_{l=1}^{4} \mathbf{D}_{2l}^{-1}(\omega) F_l(\omega) \\ \sum_{l=1}^{4} \mathbf{D}_{3l}^{-1}(\omega) F_l(\omega) \\ \sum_{l=1}^{4} \mathbf{D}_{4l}^{-1}(\omega) F_l(\omega) \end{bmatrix},$$

(92)

where $\delta J_{ext}(\omega)$ in Eq. (92) still needs to be determined. Using Eq. (57) in Eq. (61), summing over the index j, and making use of Eq. (92) yields

$$\delta V(\omega) = Z(\omega)\,\delta I_{ext}(\omega) - q\frac{\tau_{in}}{C_{inj}} \left[\frac{F_{in}(\omega)}{(1 + j\omega\,\tau_{in})} \right.$$

$$- \sum_{k=1}^{3} \sum_{l=1}^{4} \left(\frac{1}{\tau_{in}} \frac{C_{inj}}{C_k} + \frac{1}{\tau_k(1 + j\omega\,\tau_{in})} \right)$$

$$\left. \times \mathbf{D}_{kl}^{-1}(\omega) F_l(\omega) \right],$$

(93)

where $F_{in} = \Sigma_{j=1}^{N} f_{in}^j$. Substituting the value of $\delta V(\omega)$ from Eq. (69) in Eq. (93), we get the final expression for the current fluctuations $\delta I_{ext}(\omega)$ in the external circuit
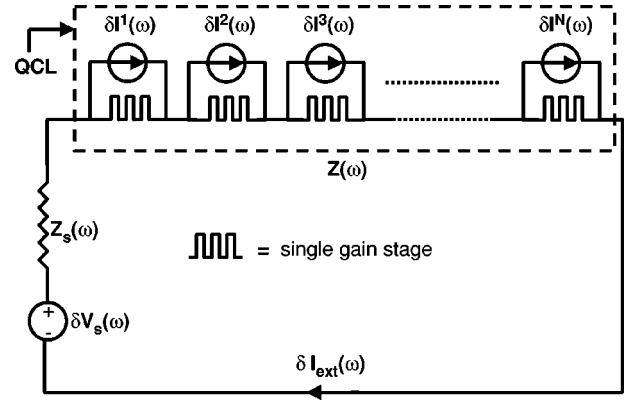

FIG. 11. Circuit model for the current fluctuations.

$$\delta I_{ext}(\omega) = \frac{\delta V_s(\omega)}{[Z(\omega) + Z_s(\omega)]}$$

$$+ \frac{q}{[Z(\omega) + Z_s(\omega)]} \frac{\tau_{in}}{C_{inj}} \left[\frac{F_{in}(\omega)}{(1 + j\omega\,\tau_{in})} \right.$$

$$- \sum_{k=1}^{3} \sum_{l=1}^{4} \left(\frac{1}{\tau_{in}} \frac{C_{inj}}{C_k} + \frac{1}{\tau_k(1 + j\omega\,\tau_{in})} \right)$$

$$\left. \times \mathbf{D}_{kl}^{-1}(\omega) F_l(\omega) \right].$$

(94)

The fluctuation $\delta P_{out}(\omega)$ in the output power can be obtained by substituting Eq. (94) in Eq. (92), and using Eq. (36)

$$\delta P_{out}(\omega) = \eta_o \frac{h\nu}{q} \frac{N}{\tau_p} \frac{\mathbf{D}_{43}^{-1}(\omega)}{(1 + j\omega\,\tau_{in})} \delta I_{ext}(\omega)$$

$$+ \eta_o \frac{h\nu}{q} \frac{WL}{\tau_p} \left[q\sum_{l=1}^{4} \mathbf{D}_{4l}^{-1}(\omega) F_l(\omega) \right] + F_o(\omega).$$

(95)

VII. CURRENT NOISE: RESULTS AND DISCUSSION

A. Circuit models for the current noise

A circuit model for the current fluctuations can be constructed by attaching a current-noise source $\delta I^j(\omega)$ in parallel with the jth gain stage, as shown in Fig. 11. But current-noise sources belonging to two different gain stages are not independent but are correlated. This is because electron densities in different gain stages interact with the same optical field. A simpler approach, more relevant from the experimental point of view, will be followed in this paper. Equation (94) for the current fluctuations in the external circuit can be written as

$$\delta I_{ext}(\omega) = \frac{\delta V_s(\omega)}{[Z(\omega) + Z_s(\omega)]} + \frac{Z(\omega)}{[Z(\omega) + Z_s(\omega)]} \delta I(\omega).$$

(96)
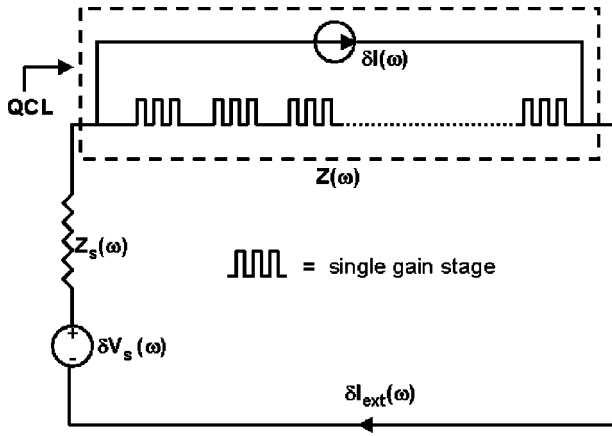
Expression for $\delta I(\omega)$ is

FIG. 12. A simplified circuit model for the current fluctuations.

$$\delta I(\omega) = \frac{q}{Z(\omega)} \frac{\tau_{in}}{C_{inj}} \left[\frac{F_{in}(\omega)}{(1+j\omega\tau_{in})} - \sum_{k=1}^{3} \sum_{l=1}^{4} \left(\frac{1}{\tau_{in}} \frac{C_{inj}}{C_k} \right.\right.$$

$$\left.\left. + \frac{1}{\tau_k(1+j\omega\tau_{in})} \right) \mathbf{D}_{kl}^{-1}(\omega) F_l(\omega) \right]. \quad (97)$$

It follows that a circuit model for the current fluctuations can be constructed by attaching a single current-noise source $\delta I(\omega)$ in parallel with all the gain stages of the QCL as shown in Fig. 12. Equation (96) shows that the current noise $\delta I(\omega)$ is equal to the current noise $\delta I_{ext}(\omega)$ in the external circuit if $\delta V_s(\omega)$ and $Z_s(\omega)$ are both zero. This is also obvious from Fig. 12. The characteristics of the noise source $\delta I(\omega)$ are explored next.

B. Spectral density and Fano factor of the current noise

The spectral density $K_I(\omega)$ of the noise source $\delta I(\omega)$ can be calculated from Eq. (97). Most of the numerical results
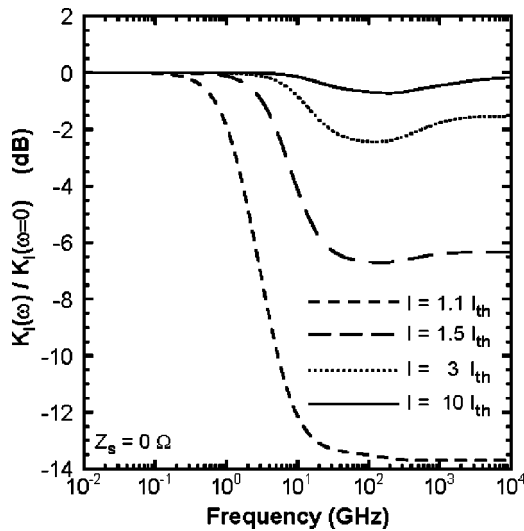

FIG. 13. Spectral density $K_I(\omega)$ of the current noise is plotted as a function of the frequency. The noise-spectral density has been normalized with respect to its value at zero frequency. For values of the QCL parameters see Table I.
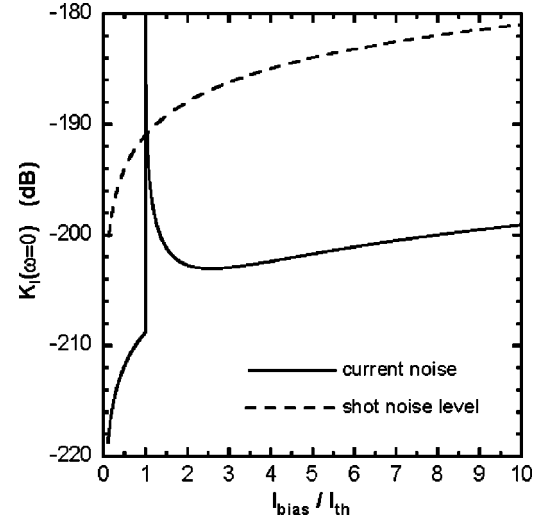

FIG. 14. Low-frequency spectral density $K_I(\omega=0)$ of the current noise is plotted as a function of the bias current. For values of the QCL parameters see Table I. The vertical scale in dB is Amp^2/Hz.

presented in this paper, unless stated otherwise, are for the QCL described in Ref. 11. The device parameters for this QCL are given in the Table I. In the numerical calculations values of all the device time constants (except τ_{st}) were assumed to be independent of bias. The values of χ_{in} and χ_{out} were assumed to be unity (see the discussion in Sec. V B). Figure 13 shows the frequency dependence of $K_I(\omega)$ for different values of the bias current. As expected, $K_I(\omega)$ rolls over near the 3-dB frequency (ω_{3dB}) for the laser modulation response (Fig. 14). Figure 15 shows the Fano factor (Appendix E) for the low-frequency fluctuations of the current-noise source $\delta I(\omega)$ as a function of the bias current. Near the laser threshold the current fluctuations are very large. Below threshold, the photon-number fluctuations inside the laser cavity are damped by the photon loss from the cavity. Above threshold, the photon-number fluctuations are
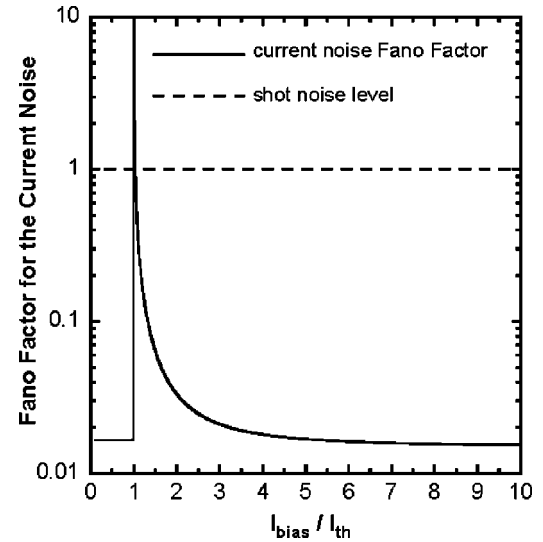

FIG. 15. Fano factor for the low-frequency current fluctuations is plotted as a function of the bias current. For values of the QCL parameters see Table I.

damped by negative feedback from the electron density in the lasing levels. Near the laser threshold, both these damping mechanisms are small and, therefore, photon-number fluctuations and, consequently, the electron-density fluctuations become large. Since, as discussed in detail below, the current fluctuations are partly driven by the electron-density

fluctuations, the current noise is also large near the laser threshold. Away from the laser threshold the current noise is suppressed far below the shot noise value.

For frequencies less than ω_{3dB}, analytical expression for $K_I(\omega)$ can be found using the expressions for the elements of the matrix $\mathbf{D}^{-1}$ given in Appendix D

$$
K_I(\omega)|_{\omega<\omega_{3dB}} =
\begin{cases}
q\dfrac{I}{N}\dfrac{\left[\chi_{in}^2+(\theta_3')^2+(\theta_2')^2\left(1+2\dfrac{\tau_{32}}{\tau_{31}}\right)+(\theta_1\chi_{out})^2\right]}{(1+\theta_3'+\theta_2'+\theta_1)^2} & (I<I_{th}) \\[4mm]
q\dfrac{I}{N}\dfrac{[\chi_{in}^2+(\theta_3+\theta_2)^2+(\theta_1\chi_{out})^2]}{(1+\theta_3+\theta_2+\theta_1)^2}+2qn_{sp}\eta_r\dfrac{(I-I_{th})}{N}\dfrac{\left(\theta_3\dfrac{\tau_{st}}{\tau_{21}}-\theta_2\dfrac{\tau_{st}}{\tau_{31}}\right)^2}{(1+\theta_3+\theta_2+\theta_1)^2} & (I>I_{th}).
\end{cases}
\tag{98}
$$

Expressions for the parameters θ_3, θ_3', θ_2, θ_2', and θ_1 are given in Appendix B. The expression for $K_I(\omega)$ above threshold is valid provided

$$
N\Gamma v_g g - \frac{1}{\tau_p} \approx 0 \quad \text{and} \quad S_p \gg \frac{n_{sp}}{WL}.
\tag{99}
$$

It is insightful to compare the expression for the current noise in Eq. (98) to the current noise in interband semiconductor diode lasers. Using the model presented in Appendix F one gets for diode lasers (see Appendix F for details)

$$
K_I(\omega)|_{\omega<\omega_{3dB}} =
\begin{cases}
qI & (I<I_{th}) \\[4mm]
qI+2qI_{th}\dfrac{(\theta'-\theta)}{(1+\theta)}+2qn_{sp}\eta_i(I-I_{th})\dfrac{\left(\theta\dfrac{\tau_{st}}{\tau_e}\right)^2}{(1+\theta)^2} & (I>I_{th}),
\end{cases}
\tag{100}
$$

where η_i is the current-injection efficiency, θ' is a number of the order of unity, and θ is much less than unity (see Appendix F). Comparing Eqs. (98) and (100) one can see that below threshold and also much above threshold (when $\tau_{st}\to0$ and $I\gg I_{th}$) the current noise approaches the shot noise value in diode lasers, whereas in QCL's the current noise can be suppressed much below the shot noise value. The mechanisms responsible for the suppression of the current noise in QCL's are discussed below.

1. Effect of small differential impedance of a single gain stage

The total differential impedance of all the gain stages in a N-stage QCL is larger than the differential impedance of a single gain stage by a factor of N. This reduces the total noise power of the current fluctuations by a factor of N, and therefore, $K_I(\omega)$ has an explicit $1/N$ dependence in Eq. (98).

2. Effect of electronic correlations

The expression for the current fluctuations $\delta I(\omega)$ given in Eq. (97), for frequencies less than ω_{3dB}, can also be written as

$$
\frac{N\,\delta I(\omega)}{qWL} = \sum_{j=1}^{N}\left[f_{in}^j(\omega)-\sum_{k=1}^{3}\left(\frac{1}{\tau_{in}}\frac{C_{inj}}{C_k}+\frac{1}{\tau_k}\right)\delta n_k^j(\omega)\right].
\tag{101}
$$

Equation (101), which is almost identical to Eq. (F32) given in Appendix F for semiconductor diode lasers, shows that fluctuations in the electron density in different levels of the gain stage causes fluctuations in the current. The sign of the current fluctuations is such as to restore the electron density to its average value thus providing a negative feedback. The physical mechanisms responsible for this negative feedback are discussed below. On one hand, these *electronic correlations* suppress the current noise associated with electron injection into the gain stage by providing negative feedback, and on the other hand, they are also responsible for generating current noise in response to electron-density fluctuations caused by noise sources internal to the gain stage. Various physical mechanisms included in our model that contribute to these electronic correlations are described below.

(1) *Coulomb Correlations*. If the electron density changes in any level of the gain stage then the electrostatic potential energy of level 3 also changes because of Coulomb interactions. As a result, the energy-level separation $\delta E_{inj}-\delta E_3$ also changes, and consequently the total electron current from the injector into the gain stage also changes. Usually QCL's are not biased in the negative differential regime and the value of the conductance G_{in} given by Eq. (48) is positive. Therefore, the change in the current will be such as to restore the electron density in the levels of the gain stage to

its steady-state value. Coulomb correlations provide negative feedback to regulate electron-density fluctuations. If a QCL is biased in the negative differential regime, in which the Coulomb correlations provide positive feedback (negative G_{in}), the fluctuations may increase substantially and the linearized noise analysis presented in this paper may not be applicable. In our model the effect of Coulomb correlations was introduced through the parameters G_{in}/C_k' in Eq. (47).

(2) *Pauli's exclusion and backward tunneling current.* If the electron density increases in level 3 of the gain stage then this reduces the phase space available for additional electrons to tunnel into level 3 from the injector due to Pauli's exclusion, and consequently the forward tunneling current from the injector into level 3 decreases from its average value. In addition, an increase in electron density in level 3 also increases the backward tunneling current from level 3 into the injector and this also reduces the net current from the injector into level 3 [recall from Eq. (37) that the net current is the difference of the forward and backward tunneling currents]. In our model both these effects were introduced through the parameter t_3^{-1} in Eq. (47). We remind the readers that later in Eqs. (56) and (57) t_3^{-1} and G_{in}/C_3' were absorbed in the definition of τ_3^{-1}, and G_{in}/C_2' and G_{in}/C_3' were relabeled as τ_2^{-1} and τ_1^{-1}, respectively. Therefore, Coulomb correlations, Pauli's exclusion, and backward tunneling current account for the presence of the terms $\delta n_k^j(\omega)/\tau_k$ in Eq. (101).

(3) *Injector electron-density response.* Here we explain the presence of the terms $(C_{inj}/\tau_{in}C_k)\delta n_k^j(\omega)$ in Eq. (101). Recall that the current fluctuations $\delta I(\omega)$ can be evaluated by looking at the current fluctuations $\delta I_{ext}(\omega)$ in the external circuit when $Z_s(\omega)$ is zero and all external voltage sources are incrementally shorted, and the sum of the fluctuations in voltage across all the gain stages (i.e., $\Sigma_{j=1}^N \delta V^j$) is, therefore, also zero. Under these conditions the relationship between the fluctuations in the carrier densities, expressed earlier in Eq. (44), becomes

$$\sum_{j=1}^{N} \delta n_{inj}^j(\omega) = -\sum_{j=1}^{N} \sum_{k=1}^{3} \frac{C_{inj}}{C_k} \delta n_k^j(\omega). \qquad (102)$$

Equation (102) can be used to write Eq. (101) as

$$\frac{N \,\delta I(\omega)}{qWL} = \sum_{j=1}^{N} \left[\frac{1}{\tau_{in}} \delta n_{inj}^j(\omega) - \sum_{k=1}^{3} \left(\frac{1}{\tau_k} \delta n_k^j(\omega) \right) + f_{in}^j(\omega) \right]. \qquad (103)$$

Equation (103) shows that the current fluctuations are proportional to the total fluctuations in the electron density in the injector states of all the stages. Since $\Sigma_{j=1}^N \delta V^j(\omega) = 0$, a net increase in the electron density in different levels of all the gain stages must result in a net decrease of the electron density in all the injector states, and consequently, the current being injected into the gain stages must also decrease. This effect is captured through the terms $(C_{inj}/\tau_{in}C_k)\delta n_k^j(\omega)$ appearing in Eq. (101).

As a result of the electronic correlations described above, the current noise associated with electron injection into the gain stages, which is represented in our model through the

noise sources $f_{in}^j(\omega)$, is suppressed. Electron-density fluctuations caused by sources internal to the gain stage contribute more strongly towards the current fluctuations because of the same correlations. To see this in a more transparent fashion it is best to write Eq. (101) in terms of all the noise sources. Below threshold, Eq. (101) becomes

$$\frac{N \,\delta I(\omega)}{qWL} = \frac{1}{(1 + \theta_3' + \theta_2' + \theta_1)} \sum_{j=1}^{N} \left[f_{in}^j(\omega) + \theta_1 f_{out}^j(\omega) \right.$$

$$+ (\theta_3' + \theta_2') f_{31}^j(\omega) + \theta_2' \left(1 + \frac{\tau_{32}}{\tau_{31}} \right) f_{21}^j(\omega)$$

$$\left. + \left(\theta_3' - \theta_2' \frac{\tau_{32}}{\tau_{31}} \right) f_{32}^j(\omega) \right]. \qquad (104)$$

Above threshold, $\delta I(\omega)$ is

$$\frac{N \,\delta I(\omega)}{q\,WL} = \frac{1}{(1 + \theta_3 + \theta_2 + \theta_1)} \sum_{j=1}^{N} \left[f_{in}^j(\omega) + \theta_1 f_{out}^j(\omega) \right.$$

$$+ (\theta_3 + \theta_2)[f_{31}^j(\omega) + f_{21}^j(\omega)] + \left(\theta_3 \frac{\tau_{st}}{\tau_{21}} - \theta_2 \frac{\tau_{st}}{\tau_{31}} \right)$$

$$\left. \times \left(f_{RS}^j(\omega) - \frac{F_L(\omega)}{N} \right) \right]. \qquad (105)$$

Note that the strength of the electronic correlations depends on the values of the parameters θ_3, θ_3', θ_2, θ_2', and θ_1 (Appendix B). From Eqs. (104) and (105) it is clear that larger values of these parameters will result in stronger electronic correlations, larger suppression of the current noise associated with electron injection into the gain stage, and also larger contribution to the current noise from the noise sources internal to the gain stage. The reader is encouraged to compare Eqs. (104) and (105) with the corresponding expressions for semiconductor diode lasers given in Eqs. (F33) and (F34) in Appendix F.

A quantitative measure of the role played by the electronic correlations in suppressing the current noise can be obtained by multiplying the Fano factor of the current noise by N. It has been mentioned earlier that a factor of $1/N$ appears in Eq. (98) because the total differential impedance of all the gain stages is larger than the differential impedance of a single gain stage by a factor of N. Therefore, multiplying the current-noise Fano factor by N removes this explicit $1/N$ dependence in the current noise and the resulting expression can only be less than unity because of electronic correlations. Figure 16 shows the current-noise Fano factor from Fig. 15 multiplied by N. Below threshold and much above threshold, N times the current-noise Fano factor is less than 0.5. This implies that electronic correlations are responsible for suppressing the current noise by a factor greater than 2. From Eq. (98), expression for the current-noise Fano factor F_I can be written as

$$N \times F_I(\omega)|_{\omega < \omega_{3\mathrm{dB}}} = \begin{cases} \dfrac{\left[\chi_{in}^2 + (\theta_3')^2 + (\theta_2')^2\left(1 + 2\dfrac{\tau_{32}}{\tau_{31}}\right) + (\theta_1\chi_{out})^2\right]}{(1+\theta_3'+\theta_2'+\theta_1)^2} & (I<I_{th}) \\[20pt] \dfrac{[\chi_{in}^2 + (\theta_3+\theta_2)^2 + (\theta_1\chi_{out})^2]}{(1+\theta_3+\theta_2+\theta_1)^2} & (I\gg I_{th}). \end{cases} \tag{106}$$

For semiconductor diode lasers, using Eq. (100), one gets

$$F_I(\omega)|_{\omega < \omega_{3\mathrm{dB}}} = 1 \quad (I<I_{th} \quad \text{and} \quad I\gg I_{th}). \tag{107}$$

At frequencies much higher than the inverse of the smallest time constant of the QCL the current noise $\delta I(\omega)$ is just the capacitive response to the various electronic transitions that occur inside the gain stages. In the limit $\omega \to \infty$, $K_I(\omega)$ is given by the expression

$$\begin{aligned} K_I(\omega)|_{\omega\to\infty} = &\, q\frac{I}{N}\left[\left(1 - \frac{C_{inj}}{C_3}\right)^2\chi_{in}^2 + \left(\frac{C_{inj}}{C_1}\right)^2\chi_{out}^2\right] \\ &+ \frac{q^2 WL}{N}\left[R_{31}\left(\frac{C_{inj}}{C_3} - \frac{C_{inj}}{C_1}\right)^2\right. \\ &+ R_{21}\left(\frac{C_{inj}}{C_2} - \frac{C_{inj}}{C_1}\right)^2 \\ &+\left. R_{32}\left(\frac{C_{inj}}{C_3} - \frac{C_{inj}}{C_2}\right)^2\right] \quad (I<I_{th}). \tag{108} \end{aligned}$$

Above threshold, an extra term

$$q(2n_{sp}-1)n_r\frac{(I-I_{th})}{N}\left(\frac{C_{inj}}{C_3} - \frac{C_{inj}}{C_2}\right)^2 \tag{109}$$

is added to the above equation to account for the stimulated transitions. Semiconductor diode lasers, on the other hand, are charge neutral. Therefore, in the limit $\omega\to\infty$, the current
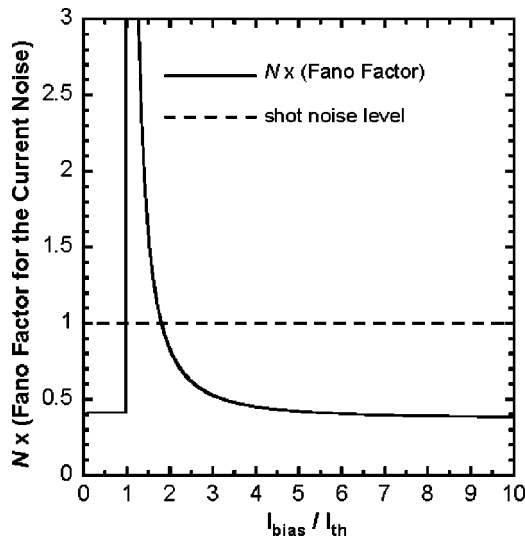

FIG. 16. N times the Fano factor for the low-frequency current fluctuations is plotted as a function of the bias current. For values of the QCL parameters see Table I.

noise in diode lasers is just the noise associated with carrier injection into the active region (see Appendix F)

$$K_I(\omega)|_{\omega\to\infty} = \begin{cases} qI(1+2\theta') & (I<I_{th}) \\ qI(1+2\theta) + 2qI_{th}(\theta'-\theta) & (I>I_{th}). \end{cases} \tag{110}$$

C. Scaling of the current noise with the number of cascade stages

In QCL's spectral density $K_I(\omega)$ of the current noise obeys a simple scaling relation with respect to the number of cascaded gain stages N and this relation can be determined from Eq. (97)

$$N^2 K_I(\omega, I/I_{th}, N) = N'^2 K_I(\omega, I/I_{th}, N'). \tag{111}$$

According to the above equation, the spectral density of the current noise, when expressed as a function of I/I_{th}, scales as $1/N^2$. This scaling relation for $K_I(\omega)$ holds for all frequencies provided that the transition rates $R_{jk}(n_j, n_k)$ and the material gain $g(n_3, n_2)$ are linear functions of the electron densities and the total mode-confinement factor also scales linearly with the number of cascade stages N.

D. Spectral density of the current noise in the external circuit

Equation (95) shows that the quantity that affects the photon noise is not the current noise $\delta I(\omega)$ but the current noise in the external circuit $\delta I_{ext}(\omega)$. When $Z_s(\omega)\neq 0$ Ω, which is usually the case, then $K_{I_{ext}}(\omega)$ is not the same as $K_I(\omega)$. Expression for $K_{I_{ext}}(\omega)$ follows from Eq. (96)

$$\begin{aligned} K_{I_{ext}}(\omega) = &\, \frac{K_{V_s}(\omega)}{|Z(\omega)+Z_s(\omega)|^2} + \left|\frac{Z(\omega)}{Z(\omega)+Z_s(\omega)}\right|^2 K_I(\omega) \\[10pt] = &\, \frac{2K_BT\,\mathrm{Re}\{Z_s(\omega)\}}{|Z(\omega)+Z_s(\omega)|^2} + \left|\frac{Z(\omega)}{Z(\omega)+Z_s(\omega)}\right|^2 K_I(\omega). \end{aligned} \tag{112}$$

Equation (112) shows that in the presence of a large impedance $Z_s(\omega)$ the current fluctuations in the external circuit are suppressed. The total differential impedance of a QCL is usually less than 1 Ω. Therefore, for even a moderately large impedance $Z_s(\omega)$ the current noise in the external circuit can be dominated by the thermal noise from the impedance $Z_s(\omega)$. Experimental measurement of the current noise would, therefore, require a relatively sensitive measurement scheme. High-impedance suppression of the current noise in
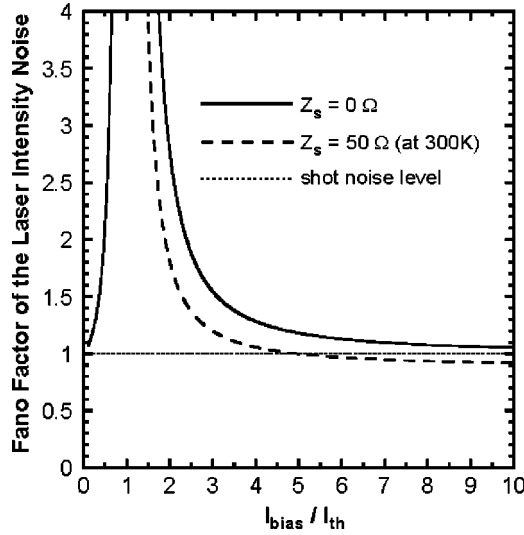
FIG. 17. Fano factor for the (low-frequency) noise in the laser intensity is plotted as a function of the bias current. For values of the QCL parameters see Table I.

the external circuit can influence the laser intensity noise, as shown in the following section.

VIII. PHOTON NOISE: RESULTS AND DISCUSSION

A. Spectral density and Fano factor of the laser intensity noise

The spectral density $K_P(\omega)$ of the intensity noise can be calculated from Eq. (95). The Fano factor for the low-frequency fluctuations in the laser output power is plotted as a function of the bias current in Fig. 17. The numerical results presented here are for the QCL structure described in Ref. 11 (see Table I). The relative intensity noise (RIN) is plotted in Fig. 18. In each figure the respective shot noise limit is also shown. It is assumed that the light coming out
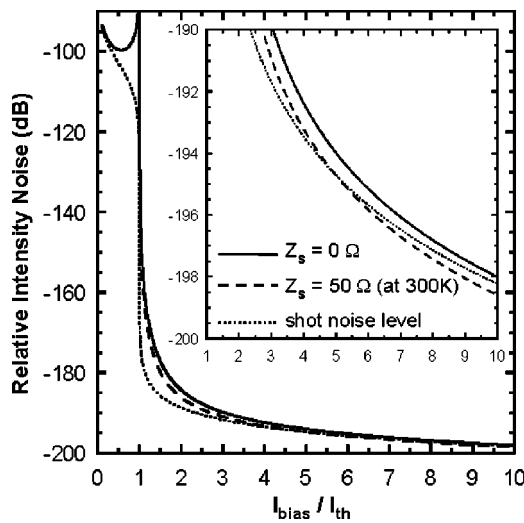

FIG. 18. Low-frequency relative intensity noise (RIN) is plotted as a function of the bias current. Very small amount of squeezing (less than 0.4 dB) is exhibited at high bias levels even when the circuit-current fluctuations are suppressed with a 50-Ω impedance. For values of the QCL parameters see Table I.
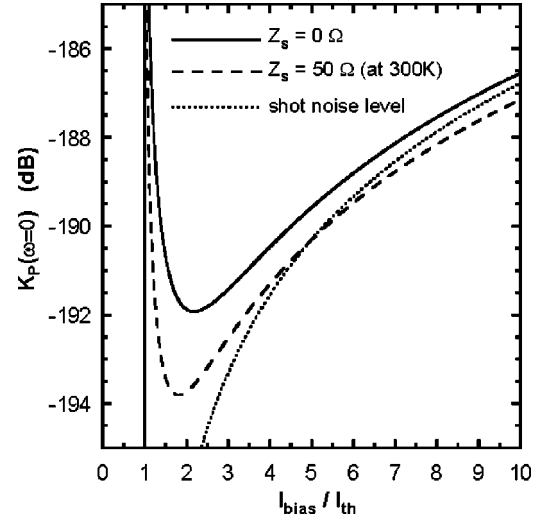

FIG. 19. Low-frequency spectral density $K_P(\omega=0)$ of the laser-intensity fluctuations is plotted as a function of the bias current. When Z_s is large (50 Ω) small amount of squeezing is seen at high bias levels. For values of the QCL parameters see Table I. The vertical scale in dB is Watt^2/Hz.

from both the facets of the laser is collected before the noise is evaluated. This is equivalent to assuming that the output coupling efficiency η_o, defined earlier in Eq. (7), is

$$\eta_o = \frac{\alpha_m}{(\alpha_m + \alpha_i)}. \tag{113}$$

In practice this can be achieved by high-reflection and anti-reflection coatings on the laser facets so that most of the light comes out from only one facet of the laser. When the value of the external impedance Z_s is 0 Ω, the photon noise remains above the shot-noise limit (Fig. 19). Even at high bias levels no amplitude squeezing is observed despite the fact that the current noise is suppressed much below the shot-noise value as shown earlier in Fig. 15. When $Z_s = 50$ Ω, and the current noise in the circuit is further suppressed, a very small amount of squeezing is observed at high bias levels (less than 0.4 dB at $I = 10\,I_{TH}$).

Figure 20 shows the RIN as a function of the frequency for different values of the bias current assuming $Z_s(\omega) = 0$. The RIN also rolls over at the frequency ω_{3dB}. Figure 21 shows that the Fano factor for the laser intensity noise as a function of the frequency. As in all other lasers, at frequencies much higher than the inverse of the photon lifetime inside the cavity, the RIN is dominated by the noise from photon partition at the output facet. Therefore,

$$K_P(\omega)\big|_{\omega \gg 1/\tau_p} = h\nu\, P_{out}. \tag{114}$$

In this paper careful attention has been given to modeling the current fluctuations in the external circuit. The question arises if such detailed modeling of the current fluctuations is necessary for calculating the photon intensity noise. In Eq. (95) the current noise $\delta I_{ext}(\omega)$ is included in the first term on the right-hand side. It should be noted here that the first and the second term on the right-hand side in Eq. (95) are correlated and the spectral density of the photon noise cannot
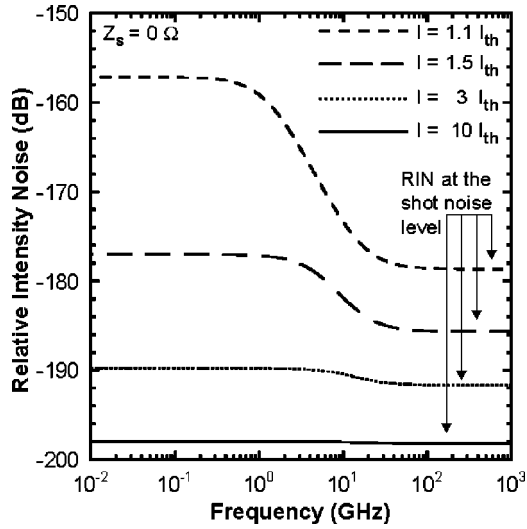
FIG. 20. Relative intensity noise (RIN) is plotted as a function of the frequency for different bias currents ($Z_s = 0 \, \Omega$). At high frequencies the RIN reaches the shot noise value. For values of the QCL parameters see Table I.

be obtained by a simple addition of the spectral densities of these two terms. In Fig. 22 the ratio of the low-frequency spectral density of the photon intensity noise obtained by ignoring the term containing $\delta I_{ext}(\omega)$ in Eq. (95) to the actual spectral density of the photon intensity noise is plotted as a function of the bias current for different values of the impedance Z_s. When the laser is biased a little above threshold the fluctuations in the current are large and the error incurred by ignoring the term containing $\delta I_{ext}(\omega)$ in Eq. (95) is also large. Also, when Z_s is much larger than the total differential impedance of the QCL, the current fluctuations in the circuit are suppressed and the term containing $\delta I_{ext}(\omega)$ can be ignored in Eq. (95).
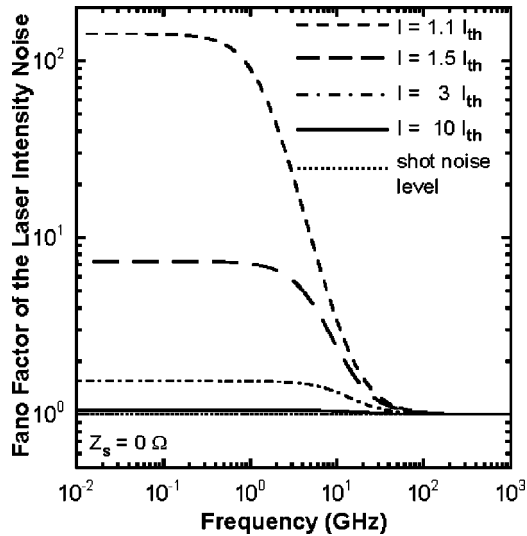

FIG. 21. Fano factor for the laser intensity noise is plotted as a function of the frequency ($Z_s = 0 \, \Omega$). The intensity noise at frequencies much higher than the inverse of the photon lifetime in the cavity is dominated by the photon partition noise at the output facet. For values of the QCL parameters see Table I.
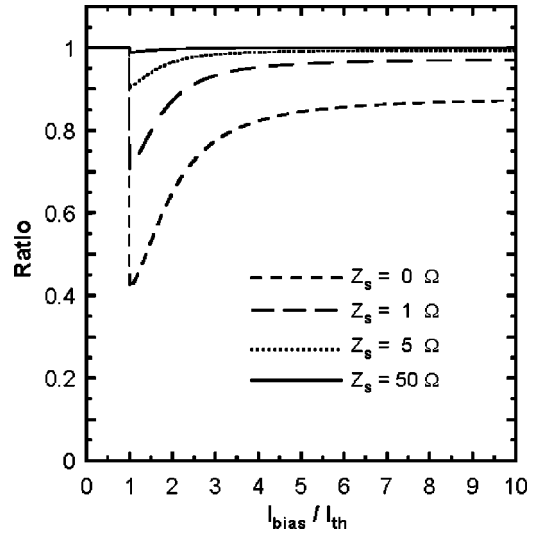

FIG. 22. Ratio of the low-frequency photon-noise-spectral density obtained by ignoring the term containing the current fluctuations in Eq. (95) to the actual spectral density is plotted as a function of the bias current for different values of the impedance Z_s. The current fluctuations are suppressed when Z_s is large and the error incurred in calculating the spectral density is, therefore, small. For values of the QCL parameters see Table I.

For large $Z_s(\omega)$, using the expressions for the elements of the matrix $\mathbf{D}^{-1}$ in Appendix D, analytical expression can be obtained for the spectral density of the low-frequency intensity noise

$$K_P(\omega)\big|_{\omega < \omega_{3dB}} = h\nu P_{out} \left[1 - \eta_o + 2\eta_o n_{sp} \left(\frac{\tau_{31}}{\tau_{21} + \tau_{31}} \right)^2 \right.$$
$$\times \left(\frac{1}{\tau_{31}} + \frac{1}{\tau_{32}} \right)^2 \tau_{st}^2 \left. \right] + (\eta_o h\nu)^2 NWL[R_{32}$$
$$+ \eta_r^2 R_{31} + (1 - \eta_r)^2 R_{21}] \qquad (115)$$

$$= h\nu P_{out} \left[1 - \eta_o + 2\eta_o n_{sp} \left(\frac{\tau_{31}}{\tau_{21} + \tau_{31}} \right)^2 \left(\frac{1}{\tau_{31}} \right.\right.$$
$$\left.\left. + \frac{1}{\tau_{32}} \right)^2 \tau_{st}^2 \right] + (\eta_o h\nu)^2 N \left[\alpha \frac{I}{q} + \beta \frac{I_{th}}{q} \right].$$
$$\qquad (116)$$

η_r in the above equation is the radiative efficiency defined in Eq. (31). The constants α and β are

$$\alpha = \eta_r(1 - \eta_r) + 2(1 - \eta_r)\frac{\tau_{31}}{\tau_{21} + \tau_{31}} \left(\frac{\tau_{21}}{\tau_{32}} \right), \qquad (117)$$

$$\beta = \eta_r - 2\eta_r(1 - \eta_r)\frac{\tau_{32}}{\tau_{31} + \tau_{32}}. \qquad (118)$$

The above expression for $K_P(\omega)$ is valid for frequencies smaller than ω_{3dB} and when the laser is biased above threshold then the conditions given by Eq. (99) are satisfied. The expression given in Eq. (116) is almost identical to the expression for $K_P(\omega)$ for semiconductor diode lasers (when the latter are also biased with a high-impedance current source).

Using the model presented in Appendix F one gets for diode lasers (see Appendix F for details)

$$K_P(\omega)|_{\omega<\omega_{3dB}}=h\nu P_{out}\left[1-\eta_o+2\eta_o n_{sp}\left(\frac{1}{\tau_w}+\frac{1-\eta_i}{\tau_e}\right)^2\tau_{st}^2\right]$$

$$+(\eta_o h\nu)^2\left[\eta_i(1-\eta_i)\frac{I}{q}+\eta_i\frac{I_{th}}{q}\right]. \qquad (119)$$

η_i in the above equation is the current injection efficiency into the quantum wells.[21]

The contributions from the nonradiative electronic transitions to the photon noise in QCL's and diode lasers are proportional to the terms inside the second square bracket in Eqs. (115) and (119), respectively. The contributions to the photon noise from the photon loss, the laser cavity, and from the radiative transitions in QCL's and diode lasers are proportional to the terms inside the first square bracket in Eqs. (115) and (119), respectively. Two important differences emerge when Eq. (115) is compared to Eq. (119) and both these differences make it harder to achieve photon-number squeezing in QCL's compared to diode lasers. These differences are discussed in detail below.

1. Contribution of nonradiative transitions to photon noise

The contribution to the photon noise from the nonradiative recombination in diode lasers is constant above threshold and it has been expressed in terms of the threshold current in Eq. (119). As shown earlier, in QCL's above threshold the electron densities in different energy levels of a gain stage do not remain fixed at their threshold values. The electron densities keep increasing when the bias current is increased beyond threshold. As a result, the contribution of nonradiative electronic transitions to the photon noise also keeps increasing with the bias current. Since only a fraction η_r of the electrons injected in level 3 of the gain stage end up producing photons, a multiplicative factor η_r^2 appears with the transition rate R_{31} in Eq. (115). A fraction $1-\eta_r$ of the vacancies left by removing electrons from level 2 get filled by radiative transitions from level 3 to level 2 and therefore a factor $(1-\eta_r)^2$ appears with R_{21}. All the electrons taken out of level 2 and injected into level 3 will end up producing photons (since $1-\eta_r+\eta_r=1$) and, therefore, R_{32} has no multiplicative factor in Eq. (115).

The noise associated with the electron transitions from level 1 into the injector of the next stage does not directly contribute to photon noise at low frequencies. These transitions contribute to the current noise in the external circuit, which can in turn contribute to the photon noise. But we have assumed in Eq. (115) that $Z_s(\omega)$ is large and the current fluctuations are suppressed. Similarly, the noise associated with the electron transitions from the injector into level 3 of the gain stage is also suppressed at low frequencies when $Z_s(\omega)$ is large.

In diode lasers, since the current injection efficiency η_i is less than unity, the partition noise associated with carrier leakage from the separate confinement heterostructure (SCH) regions contributes a term to the photon noise that increases linearly with the bias current even beyond the laser threshold, as shown in Eq. (119). Since η_i is usually close to unity in well-designed diode lasers,[21] the contribution of this term to the photon noise is small.

2. Contributions of photon loss and radiative transitions to photon noise

The most important contribution to the photon noise from the photon loss from the laser cavity and from the radiative transitions is given by the term proportional to τ_{st}^2 in Eqs. (115) and (119). Just above threshold the photon density is small and τ_{st}, which is inversely proportional to the photon density, is large. Consequently, just above threshold the term proportional to τ_{st}^2 dominates all the other terms in Eqs. (115) and (119). As the bias current is increased and the photon density becomes large, τ_{st} becomes small. It is evident from Eqs. (115) and (119) that photon number squeezing can only be achieved if the ratio $(\tau_{st}/\tau_{nr})^2$, where τ_{nr} is the total nonradiative lifetime for the carrier density interacting with the photons becomes smaller than one. The appearance of this ratio is related to the carrier density and the photon-density dynamics in response to sudden radiative transition events or photon loss events that temporarily move the carrier density and the photon density away from their steady-state values. In diode lasers τ_{nr}, given by

$$\frac{1}{\tau_{nr}}=\frac{1}{\tau_w}+\frac{1-\eta_i}{\tau_e} \quad \text{(Diode lasers)}, \qquad (120)$$

is around 500 ps (see Appendix F and Ref. 21). In QCL's, τ_{nr} is the nonradiative lifetime of the difference carrier density (n_3-n_2) that interacts with the photons and is given by the expression

$$\frac{1}{\tau_{nr}}=2\frac{\tau_{31}}{\tau_{21}+\tau_{31}}\left(\frac{1}{\tau_{31}}+\frac{1}{\tau_{32}}\right) \quad \text{(QCL's)}. \qquad (121)$$

The factor of 2 in the above equation does not show up in Eq. (115) because the differential stimulated emission lifetime of the difference carrier density is $\tau_{st}/2$ and the factor of 2 cancels out. In deriving the above equation the sum carrier density (n_3+n_2), which does not interact with the photons, was adiabatically eliminated from the rate equations. In QCL's the value of $(2\tau_{nr})$ is usually around a few picoseconds. In the QCL structure of Ref. 11, whose parameters are given in Table I, $(2\tau_{nr})$ equals 1.5 ps. Therefore, for photon-number squeezing to be possible the value of τ_{st} in QCL's must be a few hundred times less than the value of τ_{st} is diode lasers (assuming both have equal values for η_o and n_{sp}). For the same photon density and the mode group velocity the ratio of τ_{st} in QCL's and diode lasers (DL) depends on their respective differential gains [see Eqs. (80) and (F6)]. For the QCL described in Ref. 11

$$\frac{(1/\tau_{st})_{QCL}}{(1/\tau_{st})_{DL}}=\frac{aL_p}{dg/dN_w}\sim15. \qquad (122)$$

In the above equation the differential gain dg/dN_w of diode lasers is assumed to be around $(1.0–1.5)\times10^{-15}$ cm².[21] Note that the ratio in Eq. (122) is independent of any geometrical factors and depends only on the properties of the
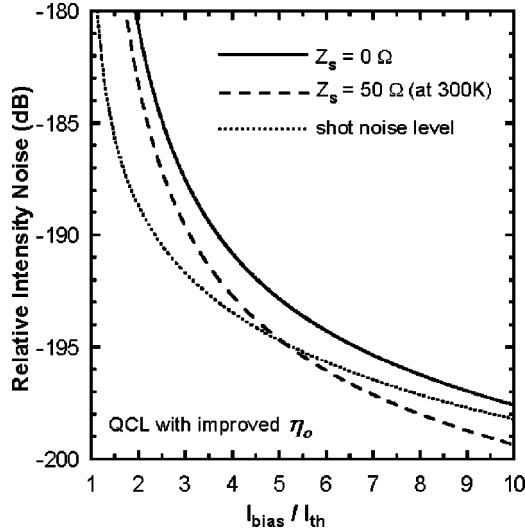
FIG. 23. Relative intensity noise (RIN) for the QCL with improved η_o ($=0.84$) is shown. Only 1.2 dB of squeezing is seen at high bias levels and when $Z_s=50\ \Omega$.

material gain of the lasers. The expression above implies that the photon density in the active region of QCL's must be at least an order of magnitude larger than the photon density in diode lasers to make squeezing possible. This does not seem to be a formidable obstacle to achieve photon-number squeezing in QCL's since QCL's with output powers exceeding 1.0 W have been demonstrated.[11] However, in QCL's, in contrast to diode lasers, it will be difficult to achieve squeezing with only a few tens of milliwatts of output power. In QCL's, since both τ_{nr} and τ_{st} depends on the spatial overlap of the wave functions of the upper and lower lasing states, it may not be possible to change the value of the ratio (τ_{st}/τ_{nr}) by engineering the wave function overlap.

The output coupling efficiency η_o of QCL's that have been reported in the literature is much smaller than those of typical diode lasers. But even if that were not the case, squeezing is expected to be less in QCL's than in diode lasers for the reasons discussed above. The QCL, whose characteristics are shown in Figs. 17 and 18, has a 3-mm long cavity, a waveguide loss of 11 cm^{-1}, and an output coupling efficiency of only 28%. Consider a QCL with a 500-μm long cavity, a waveguide loss of 5 cm^{-1}, and an output coupling efficiency of 84%, which is comparable to that of good diode lasers.[21] The values of all the other parameters of this QCL are identical to those given in Table I. Figure 23 shows the relative intensity noise when this QCL is driven with a 50 Ω resistor in series. Only about 1.2 dB of squeezing is observed even at very large bias levels ($I \approx 10\,I_{TH}$).

The Fano factors for the laser intensity noise much above threshold (when $\tau_{st} \rightarrow 0$ and $I \gg I_{th}$) in QCL's and diode lasers can be calculated from Eqs. (116) and (119),

$$F_P(\omega)\big|_{(\omega < \omega_{3dB},\, I \gg I_{th})}$$

$$= \begin{cases} 1 - \eta_o\eta_r + 2\,\eta_o\,\dfrac{(1-\eta_r)}{\eta_r}\,\dfrac{\tau_{31}}{\tau_{21}+\tau_{31}}\left(\dfrac{\tau_{21}}{\tau_{32}}\right) & \text{(QCL's)} \\[2ex] 1 - \eta_o\eta_i & \text{(Diode lasers)} \end{cases}$$

$$(123)$$

Equation (123) gives the maximum photon-number squeezing that is asymptotically achievable in QCL's and in diode lasers at very large output power levels. In real devices the squeezing will be always less than that predicted in Eq. (123). In diode lasers η_i and η_o can be larger than 0.9 and 0.85, respectively,[21] and the intensity noise in diode lasers can be maximally suppressed more than 6 dB below the shot noise value. For the QCL whose parameters are listed in Table I, η_r and η_o have the values 0.66 and 0.28, respectively, and, consequently, the maximum possible squeezing is only 0.6 dB. Even if the output coupling efficiency η_o of this QCL is increased to 0.85, the maximum squeezing predicted by Eq. (123) is only 2.0 dB.

The maximum squeezing achievable in QCL's can be increased by decreasing the lifetime τ_{21} of electrons in level 2 of the gain stage and increasing the lifetimes τ_{31} and τ_{32} associated with the nonradiative electronic transitions out of level 3. This will reduce the rate of increase of the electron density above threshold in levels 3 and 2 with the bias current, increase the radiative efficiency η_r, and reduce the contribution of the nonradiative electronic transitions to the photon noise.

B. Scaling of the laser intensity noise with the number of cascade stages

In QCL's $K_p(\omega)$ obeys a simple scaling relation with respect to the number of cascaded stages N, and this relation can easily be deduced from Eq. (95)

$$K_P(\omega, I/I_{th}, N) = K_P(\omega, I/I_{th}, N'). \qquad (124)$$

According to Eq. (124), the spectral density of the photon noise, when expressed as a function of I/I_{th}, is independent of the value of N. The scaling relation for $K_p(\omega)$ holds for all frequencies and when $Z_s(\omega)$ is very large or when $Z_s(\omega)=0\ \Omega$, provided that the transition rates $R(n_j, n_q)$ and the material gain $g(n_3, n_2)$ are linear functions of electron densities and the total mode-confinement factor also scales linearly with the number of cascaded stages N. In Ref. 23 it is shown that the total mode-confinement factor scales with the number of cascaded stages according to the expression $\sim \mathrm{erf}(0.019N)$, which is almost linear in N for $N<40$.

C. Effect of multiple longitudinal modes on the measured intensity noise

Most QCL's reported in literature lase with multiple longitudinal modes. Although the intensity noise of each longitudinal mode can be large, the intensity noise of all the modes taken together is expected to be adequately described by the single-mode analysis carried out in this paper. This is because the intensity noise in different lasing modes is negatively correlated, as it is in the case of semiconductor diode lasers.[30] However, this demands that in experiments designed to measure the intensity noise attention must also be paid to optimizing the light collection efficiency such that photons are collected from all the lasing modes, otherwise intensity noise in excess of that described by Eq. (115) can be introduced.

IX. CONCLUSION

A comprehensive model for treating noise and fluctuations in intersubband quantum cascade lasers has been presented. The current noise exhibited by QCL's is much below the shot noise value. Suppression of the current noise in QCL's is largely due to the small differential resistance of individual gain stages compared to the total differential resistance of all the cascaded gain stages. In addition, electronic correlations also suppress the current noise. However, unlike semiconductor diode lasers, current noise suppression does not lead to significant photon-number squeezing in QCL's. In QCL's the contribution to the photon noise coming from the nonradiative electronic transitions keeps increasing with bias beyond the laser threshold, and this reduces the amount of photon-number squeezing achievable in QCL's compared to semiconductor diode lasers. It has also been shown that photon noise in QCL's is squeezed at photon densities much larger than those in diode lasers.

The current modulation response of QCL's has also been investigated. It has been found that the direct-current modulation response of many QCL's that have been reported in the literature is overdamped since, in contrast to diode lasers, the photon lifetime inside the optical cavity in QCL's is usually the longest time constant. The modulation bandwidth is also limited by the inverse photon lifetime. At present, in the wavelength region of interest only quantum-well infrared photodetectors have bandwidths wide enough that they could be used to study the modulation response of QCL's. However, the current noise provides an alternate way of studying the high-speed dynamics of QCL's, and as shown in this paper, the modulation bandwidth of QCL's can be found by looking at the spectral density of the current noise in the external circuit.

Although in this paper the emphasis has been on a specific multiple quantum-well QCL structure, the theoretical methods and techniques presented in this paper can be used to study a variety of QCL's that have been reported in the literature.

APPENDIX A: CORRELATIONS AMONG THE LANGEVIN NOISE SOURCES

$$WL\langle f_{32}^j(t)f_{32}^q(t')\rangle = (R_{3\rightarrow2}+R_{2\rightarrow3})\delta_{jq}\delta(t-t')$$
$$\approx R_{32}(n_3^j,n_2^j)\delta_{jq}\delta(t-t'), \qquad (A1)$$

$$WL\langle f_{31}^j(t)f_{31}^q(t')\rangle = (R_{3\rightarrow1}+R_{1\rightarrow3})\delta_{jq}\delta(t-t')$$
$$\approx R_{31}(n_3^j,n_1^j)\delta_{jq}\delta(t-t'), \qquad (A2)$$

$$WL\langle f_{21}^j(t)f_{21}^q(t')\rangle = (R_{2\rightarrow1}+R_{1\rightarrow2})\delta_{jq}\delta(t-t')$$
$$\approx R_{21}(n_2^j,n_1^j)\delta_{jq}\delta(t-t'), \qquad (A3)$$

$$WL\langle f_{RN}^j(t)f_{RN}^q(t')\rangle = \Gamma^j v_g g(n_3^j,n_2^j)\left[(2n_{sp}-1)S_p\right.$$
$$\left.+\frac{n_{sp}}{WL}\right]\delta_{jq}\delta(t-t'), \qquad (A4)$$

$$WL\langle f_{RS}^j(t)f_{RS}^q(t')\rangle = \Gamma^j v_g g(n_3^j,n_2^j)\left[(2n_{sp}-1)S_p\right.$$
$$\left.+\frac{n_{sp}}{WL}\right]\delta_{jq}\delta(t-t'), \qquad (A5)$$

$$WL\langle f_{RS}^j(t)f_{RN}^q(t')\rangle = \Gamma^j v_g g(n_3^j,n_2^j)\left[(2n_{sp}-1)S_p\right.$$
$$\left.+\frac{n_{sp}}{WL}\right]\delta_{jq}\delta(t-t'), \qquad (A6)$$

$$WL\langle F_L(t)F_L(t')\rangle = \frac{S_p}{\tau_p}\delta(t-t'), \qquad (A7)$$

$$\langle F_o(t)F_o(t')\rangle = \eta_o(h\nu)^2\frac{WLS_p}{\tau_p}\delta(t-t'), \qquad (A8)$$

$$\langle F_o(t)F_L(t')\rangle = \eta_o h\nu\frac{S_p}{\tau_p}\delta(t-t'). \qquad (A9)$$

APPENDIX B: DIFFERENTIAL RESISTANCE OF A QCL

The expression in Eqs. (65) and (63) for the differential resistance R_d of a QCL can be put in the form

$$R_d = \begin{cases} \dfrac{N}{WL}\dfrac{\tau_{in}}{C_{inj}}(1+\theta_3'+\theta_2'+\theta_1) & (I<I_{th}), \\[2ex] \dfrac{N}{WL}\dfrac{\tau_{in}}{C_{inj}}(1+\theta_3+\theta_2+\theta_1) & (I>I_{th}). \end{cases} \qquad (B1)$$

The dimensionless parameters θ_3, θ_3', θ_2, θ_2', and θ_1 that have been used in the above equation are as follows:

$$\theta_3 = \left(\frac{1}{\tau_{in}}\frac{C_{inj}}{C_3}+\frac{1}{\tau_3}\right)\frac{\tau_{31}\tau_{21}}{(\tau_{21}+\tau_{31})},$$

$$\theta_3' = \left(\frac{1}{\tau_{in}}\frac{C_{inj}}{C_3}+\frac{1}{\tau_3}\right)\frac{\tau_{32}\tau_{31}}{(\tau_{32}+\tau_{31})}, \qquad (B2)$$

$$\theta_2 = \left(\frac{1}{\tau_{in}}\frac{C_{inj}}{C_2}+\frac{1}{\tau_2}\right)\frac{\tau_{31}\tau_{21}}{(\tau_{21}+\tau_{31})},$$

$$\theta_2' = \left(\frac{1}{\tau_{in}}\frac{C_{inj}}{C_2}+\frac{1}{\tau_2}\right)\frac{\tau_{31}\tau_{21}}{(\tau_{32}+\tau_{31})}, \qquad (B3)$$

$$\theta_1 = \left(\frac{1}{\tau_{in}}\frac{C_{inj}}{C_1}+\frac{1}{\tau_1}\right)\tau_{out}. \qquad (B4)$$

APPENDIX C: ELEMENTS OF MATRIX D

The nonzero elements of the matrix **D** are

$$\mathbf{D}_{11}=j\omega+\frac{1}{\tau_{out}}, \quad \mathbf{D}_{12}=-\frac{1}{\tau_{21}}, \quad \mathbf{D}_{13}=-\frac{1}{\tau_{31}}, \quad \text{(C1)}$$

$$\mathbf{D}_{22}=j\omega+\frac{1}{\tau_{21}}+\Gamma v_g a\left(S_p+\frac{n_{sp}}{WL}\right), \quad \text{(C2)}$$

$$\mathbf{D}_{23}=-\frac{1}{\tau_{32}}-\Gamma v_g a\left(S_p+\frac{n_{sp}}{WL}\right), \quad \text{(C3)}$$

$$\mathbf{D}_{24}=-\mathbf{D}_{34}=-N\Gamma v_g g(n_3,n_2), \quad \text{(C4)}$$

$$\mathbf{D}_{31}=\frac{1}{\tau_1}\frac{j\omega\tau_{in}}{(1+j\omega\tau_{in})}, \quad \text{(C5)}$$

$$\mathbf{D}_{32}=\frac{1}{\tau_2}\frac{j\omega\tau_{in}}{(1+j\omega\tau_{in})}-\Gamma v_g a\left(S_p+\frac{n_{sp}}{WL}\right), \quad \text{(C6)}$$

$$\mathbf{D}_{33}=j\omega+\frac{1}{\tau_3}\frac{j\omega\tau_{in}}{(1+j\omega\tau_{in})}+\frac{1}{\tau_{32}}+\frac{1}{\tau_{31}}+\Gamma v_g a\left(S_p+\frac{n_{sp}}{WL}\right), \quad \text{(C7)}$$

$$\mathbf{D}_{42}=-\mathbf{D}_{43}=\Gamma v_g a\left(S_p+\frac{n_{sp}}{WL}\right), \quad \text{(C8)}$$

$$\mathbf{D}_{44}=j\omega+\frac{1}{\tau_p}-N\Gamma v_g g(n_3,n_2). \quad \text{(C9)}$$

APPENDIX D: IMPORTANT ELEMENTS OF MATRIX $\mathbf{D}^{-1}$

Above threshold, elements of the matrix $\mathbf{D}^{-1}$ in the limit $\{\tau_2,\tau_1\}\to\infty$ are given below. In addition, it is also assumed that $\omega\tau_{in}\ll1$. If the latter condition does not hold then the expressions given below can be corrected by replacing τ_3 by $\tau_3(1+j\omega\tau_{in})$.

$$\mathbf{D}_{11}^{-1}=\frac{\tau_{out}}{(j\omega\tau_{out}+1)}, \quad \text{(D1)}$$

$$\mathbf{D}_{12}^{-1}=\tau_{out}\tau_p\tau_{st}\left\{(j\omega)^2\left(1+\frac{\tau_{in}}{\tau_3}\right)\frac{1}{\tau_{21}}+j\omega\left[\frac{1}{\tau_{st}}\left(\frac{1}{\tau_{21}}+\frac{1}{\tau_{31}}\right)\right.\right.$$
$$\left.\left.+\frac{1}{\tau_{21}\tau_{31}}+\frac{1}{\tau_{21}\tau_{32}}\right]+\frac{1}{\tau_p\tau_{st}}\left(\frac{1}{\tau_{21}}+\frac{1}{\tau_{31}}\right)\right\}$$
$$\times\frac{\tau_{21}\tau_{31}}{(\tau_{21}+\tau_{31})}\frac{H(\omega)}{(j\omega\tau_{out}+1)}, \quad \text{(D2)}$$

$$\mathbf{D}_{13}^{-1}=\tau_{out}\tau_p\tau_{st}\left\{(j\omega)^2\left(\frac{1}{\tau_{31}}\right)+j\omega\left[\frac{1}{\tau_{st}}\left(\frac{1}{\tau_{21}}+\frac{1}{\tau_{31}}\right)+\frac{1}{\tau_{21}\tau_{31}}\right.\right.$$
$$\left.\left.+\frac{1}{\tau_{21}\tau_{32}}\right]+\frac{1}{\tau_p\tau_{st}}\left(\frac{1}{\tau_{21}}+\frac{1}{\tau_{31}}\right)\right\}\frac{\tau_{21}\tau_{31}}{(\tau_{21}+\tau_{31})}$$
$$\times\frac{H(\omega)}{(j\omega\tau_{out}+1)}, \quad \text{(D3)}$$

$$\mathbf{D}_{14}^{-1}=\tau_{out}\tau_{st}\left\{j\omega\left[\frac{1}{\tau_{21}}\left(1+\frac{\tau_{in}}{\tau_3}\right)-\frac{1}{\tau_{31}}\right]\right\}$$
$$\times\frac{\tau_{21}\tau_{31}}{(\tau_{21}+\tau_{31})}\frac{H(\omega)}{(j\omega\tau_{out}+1)}, \quad \text{(D4)}$$

$$\mathbf{D}_{21}^{-1}\approx0, \quad \text{(D5)}$$

$$\mathbf{D}_{22}^{-1}=\tau_p\tau_{st}\left[(j\omega)^2\left(1+\frac{\tau_{in}}{\tau_3}\right)+j\omega\left(\frac{1}{\tau_{32}}+\frac{1}{\tau_{31}}+\frac{1}{\tau_{st}}\right)\right.$$
$$\left.+\frac{1}{\tau_p\tau_{st}}\right]\frac{\tau_{21}\tau_{31}}{(\tau_{21}+\tau_{31})}H(\omega), \quad \text{(D6)}$$

$$\mathbf{D}_{23}^{-1}=\tau_p\left[j\omega\left(\frac{\tau_{st}}{\tau_{32}}+1\right)+\frac{1}{\tau_p}\right]\frac{\tau_{21}\tau_{31}}{(\tau_{21}+\tau_{31})}H(\omega), \quad \text{(D7)}$$

$$\mathbf{D}_{24}^{-1}=\tau_{st}\left[j\omega\left(1+\frac{\tau_{in}}{\tau_3}\right)+\frac{1}{\tau_{31}}\right]\frac{\tau_{21}\tau_{31}}{(\tau_{21}+\tau_{31})}H(\omega), \quad \text{(D8)}$$

$$\mathbf{D}_{31}^{-1}\approx0, \quad \text{(D9)}$$

$$\mathbf{D}_{32}^{-1}=\tau_p\left(j\omega+\frac{1}{\tau_p}\right)\frac{\tau_{21}\tau_{31}}{(\tau_{21}+\tau_{31})}H(\omega), \quad \text{(D10)}$$

$$\mathbf{D}_{33}^{-1}=\tau_p\tau_{st}\left[(j\omega)^2+j\omega\left(\frac{1}{\tau_{21}}+\frac{1}{\tau_{st}}\right)\right.$$
$$\left.+\frac{1}{\tau_p\tau_{st}}\right]\frac{\tau_{21}\tau_{31}}{(\tau_{21}+\tau_{31})}H(\omega), \quad \text{(D11)}$$

$$\mathbf{D}_{34}^{-1}=-\tau_{st}\left(j\omega+\frac{1}{\tau_{21}}\right)\frac{\tau_{21}\tau_{31}}{(\tau_{21}+\tau_{31})}H(\omega), \quad \text{(D12)}$$

$$\mathbf{D}_{41}^{-1}\approx0, \quad \text{(D13)}$$

$$\mathbf{D}_{42}^{-1}=-\tau_p\left[j\omega\left(1+\frac{\tau_{in}}{\tau_3}\right)+\left(\frac{1}{\tau_{31}}+\frac{1}{\tau_{32}}\right)\right]\frac{\tau_{21}\tau_{31}}{(\tau_{21}+\tau_{31})}H(\omega), \quad \text{(D14)}$$

$$\mathbf{D}_{43}^{-1}=\tau_p\left[j\omega+\left(\frac{1}{\tau_{21}}-\frac{1}{\tau_{32}}\right)\right]\frac{\tau_{21}\tau_{31}}{(\tau_{21}+\tau_{31})}H(\omega), \quad \text{(D15)}$$

$$\mathbf{D}_{44}^{-1} = \tau_p \tau_{st} \Biggl\{ (j\omega)^2 \left(1 + \frac{\tau_{in}}{\tau_3} \right) + (j\omega) \left[\frac{1}{\tau_{21}} \left(1 + \frac{\tau_{in}}{\tau_3} \right) + \frac{1}{\tau_{31}} \right.$$

$$+ \frac{1}{\tau_{32}} + \frac{1}{\tau_{st}} \left(2 + \frac{\tau_{in}}{\tau_3} \right) \Biggr] + \left[\frac{1}{\tau_{st}} \left(\frac{1}{\tau_{21}} + \frac{1}{\tau_{31}} \right) + \frac{1}{\tau_{21}\tau_{31}} \right.$$

$$+ \left. \frac{1}{\tau_{21}\tau_{32}} \right] \Biggr\} \frac{\tau_{21}\tau_{31}}{(\tau_{21}+\tau_{31})} H(\omega), \tag{D16}$$

where $H(\omega)$ is

$$H(\omega) = \frac{1}{\tau_p \tau_{st}} \left(\frac{1}{\tau_{21}} + \frac{1}{\tau_{31}} \right) \Biggl\{ (j\omega)^3 \left(1 + \frac{\tau_{in}}{\tau_3} \right)$$

$$+ (j\omega)^2 \left[\frac{1}{\tau_{21}} \left(1 + \frac{\tau_{in}}{\tau_3} \right) + \frac{1}{\tau_{31}} + \frac{1}{\tau_{32}} + \frac{1}{\tau_{st}} \left(2 + \frac{\tau_{in}}{\tau_3} \right) \right]$$

$$+ j\omega \left[\frac{1}{\tau_{st}} \left(\frac{1}{\tau_{21}} + \frac{1}{\tau_{31}} \right) + \frac{1}{\tau_{21}\tau_{31}} + \frac{1}{\tau_{21}\tau_{32}} \right.$$

$$+ \left. \frac{1}{\tau_p \tau_{st}} \left(2 + \frac{\tau_{in}}{\tau_3} \right) \right] + \frac{1}{\tau_p \tau_{st}} \left(\frac{1}{\tau_{21}} + \frac{1}{\tau_{31}} \right) \Biggr\}^{-1}. \tag{D17}$$

For small values of ω for which the cubic term in ω in the denominator may be neglected, $H(\omega)$ becomes

$$H(\omega) = \frac{\omega_R^2}{(\omega_R^2 - \omega^2 + j\omega\gamma)}. \tag{D18}$$

The above approximation will be valid if ω is much less than $1/\tau_{in}$, $1/\tau_{21}$, and $1/\tau_{st}$. In this approximation ω_R and γ are

$$\omega_R^2 = \frac{\dfrac{1}{\tau_p \tau_{st}} \left(1 + \dfrac{\tau_{21}}{\tau_{31}} \right)}{\left[1 + \dfrac{\tau_{21}}{\tau_{31}} + \dfrac{\tau_{21}}{\tau_{32}} + \dfrac{\tau_{in}}{\tau_3} + \dfrac{\tau_{21}}{\tau_{st}} \left(2 + \dfrac{\tau_{in}}{\tau_3} \right) \right]}, \tag{D19}$$

$$\gamma = \frac{\left[\dfrac{1}{\tau_{st}} \left(1 + \dfrac{\tau_{21}}{\tau_{31}} \right) + \dfrac{1}{\tau_{31}} + \dfrac{1}{\tau_{32}} + \dfrac{\tau_{21}}{\tau_p \tau_{st}} \left(2 + \dfrac{\tau_{in}}{\tau_3} \right) \right]}{\left[1 + \dfrac{\tau_{21}}{\tau_{31}} + \dfrac{\tau_{21}}{\tau_{32}} + \dfrac{\tau_{in}}{\tau_3} + \dfrac{\tau_{21}}{\tau_{st}} \left(2 + \dfrac{\tau_{in}}{\tau_3} \right) \right]}. \tag{D20}$$

APPENDIX E: NOISE-SPECTRAL DENSITIES AND FANO FACTORS

The spectral densities $K_I(\omega)$ and $K_P(\omega)$ of noise power for the current noise and the intensity noise, respectively, can be computed from the equations

$$K_I(\omega) = \int_{-\infty}^{\infty} \frac{d\omega'}{2\pi} \langle \delta I^*(\omega) \delta I(\omega - \omega') \rangle, \tag{E1}$$

$$K_P(\omega) = \int_{-\infty}^{\infty} \frac{d\omega'}{2\pi} \langle \delta P_{out}^*(\omega) \delta P_{out}(\omega - \omega') \rangle. \tag{E2}$$

Equations (E1) and (E2) can be used with Eqs. (97) and (95) to compute the noise-spectral densities. Since all the Langevin noise sources are δ-correlated in time domain, they will
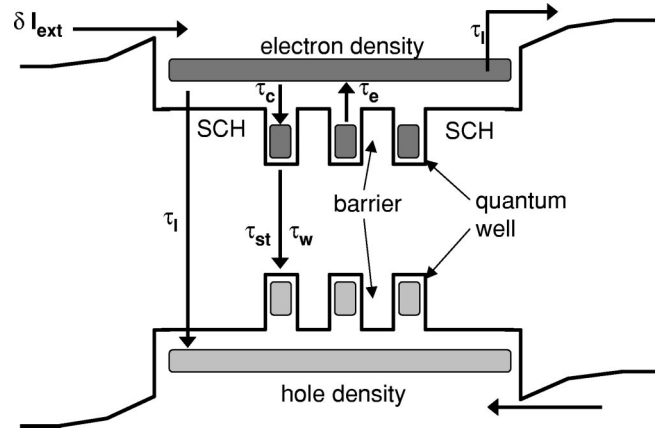

FIG. 24. Active region of a semiconductor quantum-well diode laser.

also be δ-correlated in frequency domain, and therefore, the fluctuations δI and δP_{out} in the current and the output power, respectively, will also be δ correlated in time and frequency domains.

The Fano factors $F_I(\omega)$ and $F_P(\omega)$ for the current noise and the intensity noise, respectively, are defined as the ratios of the actual noise-spectral densities to the noise-spectral densities of shot noise, and are given by the relations,

$$F_I(\omega) = \frac{K_I(\omega)}{qI} \quad \text{and} \quad F_P(\omega) = \frac{K_P(\omega)}{h\nu P_{out}}. \tag{E3}$$

The RIN is defined as

$$\text{RIN} = 10 \log_{10} \left[\frac{K_P(\omega)}{P_{out}^2} \right]. \tag{E4}$$

APPENDIX F: NOISE MODEL FOR SEMICONDUCTOR QUANTUM-WELL DIODE LASERS

A simple model for the current and photon noise in quantum-well interband semiconductor diode lasers is presented.[5,31] The active region of a quantum-well diode laser is shown in Fig. 24. The carriers are injected from the leads into the SCH region either by tunneling or by thermionic emission over the heterobarrier. The rate equations for the fluctuations δN_c and δN_w in the carrier densities (cm^{-3}), the SCH region, and the quantum wells, respectively, and the fluctuations δS_p in the photon density (cm^{-3}) are[5,31]

$$\frac{d\delta N_c}{dt} = \frac{\delta I_{ext}}{qV_c} - \delta N_c \left(\frac{1}{\tau_c} + \frac{1}{\tau_l} \right) + \frac{\delta N_w}{\tau_e} \frac{V_w}{V_c} - F_c - F_l + F_e \frac{V_w}{V_c}, \tag{F1}$$

$$\frac{d\delta N_w}{dt} = \frac{\delta N_c}{\tau_c} \frac{V_c}{V_w} - \delta N_w \left(\frac{1}{\tau_e} + \frac{1}{\tau_w} + \frac{1}{\tau_{st}} \right) - v_g g \delta S_p$$

$$+ F_c \frac{V_c}{V_w} - F_e - F_{nr} - F_{RN}, \tag{F2}$$

$$\frac{d\,\delta S_p}{dt}=\frac{\delta N_w}{\tau_{st}}\frac{V_w}{V_p}+\left(\Gamma v_g g-\frac{1}{\tau_p}\right)\delta S_p+F_{RS}-F_L, \quad \text{(F3)}$$

and the current and the intensity fluctuations are given as[5,32]

$$\frac{\delta I_{ext}}{qV_c}=\frac{G\,\delta V_d}{qV_c}-\frac{\delta N_c}{\tau_G}+F_{in}, \quad \text{(F4)}$$

$$\delta P_{out}=\eta_o h\nu\frac{V_p\delta S_p}{\tau_p}+F_o. \quad \text{(F5)}$$

It is assumed that the carrier density N_c in the SCH region also includes the carriers inside the quantum-well barriers and also those in the quantum wells that have energy high enough to not be confined within the quantum wells (Fig. 24). Only those carriers that are confined within the quantum wells are included in the carrier density N_w. V_c and V_w are the volumes of the SCH region and the quantum wells, respectively. V_p is the volume of the optical mode. τ_c and τ_e are the capture and emission times for electrons going into and coming out of the quantum wells, respectively. τ_l is the lifetime associated with carrier leakage and recombination in the SCH region. τ_w is the nonradiative recombination time in the quantum wells. τ_{st}, given by

$$\frac{1}{\tau_{st}}=v_g\frac{dg}{dN_w}\left(S_p+\frac{n_{sp}}{V_p}\right), \quad \text{(F6)}$$

is the differential lifetime associated with stimulated and spontaneous emission into the lasing mode. τ_p is the photon lifetime inside the laser cavity. δV_d is the fluctuation in the voltage across the active region. The conductance G relates the increase in the injection current into the SCH region from the leads with the increase in the voltage across the active region at a *fixed carrier density*. τ_G relates the decrease in the current injection rate to the increase in the carrier density in the SCH region. F_{in} is the Langevin noise source associated with carrier injection into the SCH region. F_l, F_c, and F_e model the noise in carrier-leakage, carrier-capture, and carrier-emission events. F_{nr} describes the noise in nonradiative recombination in the quantum wells including spontaneous emission into the nonlasing modes. F_{RN} and F_{RS} model the noise associated with photon emission into the lasing mode. F_L and F_o model the noise in photon loss from the cavity. All the nonzero correlations of the Langevin noise sources can be obtained from the methods described in Ref. 21,

$$V_c\langle F_c(t)F_c(t')\rangle=\frac{N_c}{\tau_c}\delta(t-t'), \quad \text{(F7)}$$

$$V_c\langle F_l(t)F_l(t')\rangle=\frac{N_c}{\tau_l}\delta(t-t'), \quad \text{(F8)}$$

$$V_w\langle F_e(t)F_e(t')\rangle=\frac{N_w}{\tau_e}\delta(t-t'), \quad \text{(F9)}$$

$$V_w\langle F_{nr}(t)F_{nr}(t')\rangle=\frac{N_w}{\tau_w}\delta(t-t'), \quad \text{(F10)}$$

$$V_w\langle F_{RN}(t)F_{RN}(t')\rangle=v_gg\left[(2n_{sp}-1)S_p+\frac{n_{sp}}{V_p}\right]\delta(t-t'), \quad \text{(F11)}$$

$$V_p\langle F_{RS}(t)F_{RS}(t')\rangle=\frac{V_w}{V_p}v_gg\left[(2n_{sp}-1)S_p+\frac{n_{sp}}{V_p}\right]\delta(t-t'), \quad \text{(F12)}$$

$$V_p\langle F_{RN}(t)F_{RS}(t')\rangle=v_gg\left[(2n_{sp}-1)S_p+\frac{n_{sp}}{V_p}\right]\delta(t-t'), \quad \text{(F13)}$$

$$V_p\langle F_L(t)F_L(t')\rangle=\frac{S_p}{\tau_p}\delta(t-t'), \quad \text{(F14)}$$

$$\langle F_o(t)F_o(t')\rangle=\eta_o(h\nu)^2\frac{V_pS_p}{\tau_p}\delta(t-t'), \quad \text{(F15)}$$

$$V_p\langle F_o(t)F_L(t')\rangle=\eta_o(h\nu)\frac{V_pS_p}{\tau_p}\delta(t-t'). \quad \text{(F16)}$$

F_{in} has the approximate correlation[32]

$$V_c^2\langle F_{in}(t)F_{in}(t')\rangle\approx\left(\frac{I}{q}+2\frac{N_cV_c}{\tau_G}\right)\delta(t-t'). \quad \text{(F17)}$$

The inclusion of the rate equation for fluctuations in the carrier density in the SCH region is necessary to accurately model the current noise. Carrier leakage in the SCH region results in a less than unity efficiency η_i for current injection into the quantum wells

$$\eta_i=\frac{\tau_l}{(\tau_c+\tau_l)} \quad \text{(F18)}$$

and above threshold the expression for the output power can be written as

$$P_{out}=\eta_o\eta_i\frac{h\nu}{q}(I-I_{th}), \quad \text{(F19)}$$

where η_o is the output coupling efficiency.[21]

1. Modulation response

The current modulation response of diode lasers follows from the rate equations and for frequencies less than the inverse of the carrier capture time τ_c, it can be put in the form,[21]

$$\frac{\delta P_{out}(\omega)}{\delta I_{ext}(\omega)}=\eta_o\eta_i\frac{h\nu}{q}H(\omega)=\eta_o\eta_i\frac{h\nu}{q}\frac{\omega_R^2}{(\omega_R^2-\omega^2+j\omega\gamma)} \quad \text{(F20)}$$

The relaxation oscillation frequency ω_R and the damping constant γ are

$$\omega_R^2 = \frac{\dfrac{1}{\tau_{st}\tau_p}}{1 + \eta_i \dfrac{\tau_c}{\tau_e}}, \tag{F21}$$

$$\gamma = \frac{\left(\dfrac{1}{\tau_w} + \dfrac{1-\eta_i}{\tau_e} + \dfrac{1}{\tau_{st}}\right)}{1 + \eta_i \dfrac{\tau_c}{\tau_e}} = K\omega_R^2 + \gamma_o, \tag{F22}$$

where

$$K = \tau_p \quad \text{and} \quad \gamma_o = \frac{\left(\dfrac{1}{\tau_w} + \dfrac{1-\eta_i}{\tau_e}\right)}{1 + \eta_i \dfrac{\tau_c}{\tau_e}}. \tag{F23}$$

In diode lasers, γ is small at threshold and the 3-dB frequency $\omega_{3\,dB}$ increases with the bias current until $\gamma/\sqrt{2}$ equals ω_R. As the bias current is increased beyond this point the modulation response becomes overdamped and $\omega_{3\,dB}$ starts to decrease. The maximum modulation bandwidth $\omega_{3\,dB|max}$ comes out to be

$$\omega_{3\,dB|max} \approx \frac{\sqrt{2}}{\tau_p}. \tag{F24}$$

2. Differential resistance

The differential resistance of the laser diode below and above threshold can be derived from the rate equations by removing all the noise sources

$$R_d = \begin{cases} \dfrac{1}{G}(1+\theta') & (I < I_{th}) \\[2mm] \dfrac{1}{G}(1+\theta) & (I > I_{th}), \end{cases} \tag{F25}$$

where θ' and θ are

$$\theta' = \frac{1}{\tau_G}\frac{\tau_l\tau_c}{[\tau_l(1-\eta_e)+\tau_c]}, \quad \theta = \frac{1}{\tau_G}\frac{\tau_l\tau_c}{(\tau_l+\tau_c)}, \tag{F26}$$

where the emission efficiency η_e is $\tau_w/(\tau_e+\tau_w)$. Values of the time constants τ_c, τ_e, τ_g, τ_l, and τ_w are typically 10 ps, 40 ps, 50 ps, 60 ps, and 1 ns, respectively.[34] It follows that θ' and θ have the values 0.97 and 0.17, respectively.

The discontinuity ΔR_d in the differential resistance at threshold becomes

$$\Delta R_d = \frac{1}{G}(\theta' - \theta) = \eta_i\eta_e\frac{\theta'}{G}$$

$$= \eta_i\eta_e\frac{\theta'}{1+\theta'}R_d|_{I \lesssim I_{th} \text{ evaluated at } I = I_{th}}. \tag{F27}$$

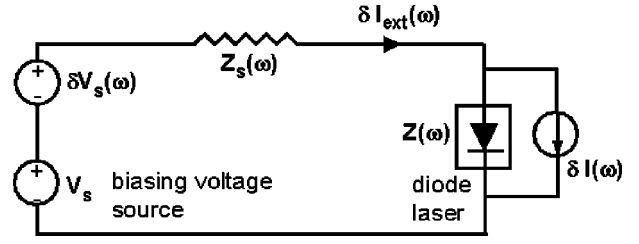Below threshold, the current-voltage characteristics of a laser diode resemble that of an ideal pn junction[33]

FIG. 25. Circuit model for the current fluctutions in semiconductor diode lasers.

$$I = I_o\left[\exp\left(\frac{qV_d}{mK_BT}\right) - 1\right], \tag{F28}$$

where m is the diode ideality factor with values usually between 1.5 and 2. Therefore,

$$R_d|_{I \leq I_{th}} = m\frac{K_BT}{qI}, \tag{F29}$$

and ΔR_d becomes

$$\Delta R_d = \eta_i\eta_e\frac{\theta'}{1+\theta'}m\frac{K_BT}{qI_{th}}. \tag{F30}$$

The above equation shows that the discontinuity in the differential resistance at threshold is K_BT/qI_{th} times a factor that is close to unity.

3. Differential impedance

The differential impedance $Z(\omega)$ of a diode laser above threshold can be expressed in terms of the modulation response $H(\omega)$

$$Z(\omega) = \frac{1}{G}\left[1 + \theta\left(1 + j\omega\eta_i\frac{\tau_p\tau_{st}}{\tau_e}H(\omega)\right)\right]. \tag{F31}$$

The differential resistance R_d above threshold, given by Eq. (F25), equals $Z(\omega = 0)$.

4. Current noise

As in the case of QCL's, the fluctuations $\delta I(\omega)$ produced by the current-noise source that sits in parallel with the laser diode (Fig. 25) can be found by looking at the current noise in the external circuit when the voltage fluctuation δV_d across the diode is zero (because all external sources and impedances are assumed to be shorted). This implies that,

$$\frac{\delta I(\omega)}{q} = V_cF_{in}(\omega) - \frac{\delta N_c(\omega)V_c}{\tau_G}. \tag{F32}$$

Below threshold, and for frequencies less than $\omega_{3\,dB}$, $\delta I(\omega)$ is

$$\frac{\delta I(\omega)}{q} = \frac{V_c F_{in}(\omega) + \theta'(1-\eta_e)[V_c F_c(\omega) - V_w F_e(\omega)] + \theta' V_c F_l(\omega) + \theta' \eta_e V_w F_{nr}(\omega)}{(1+\theta')}. \tag{F33}$$

Above threshold, $\delta I(\omega)$ is

$$\frac{\delta I(\omega)}{q} = \frac{V_c F_{in}(\omega) + \theta[V_c F_c(\omega) - V_w F_e(\omega) + V_c F_l(\omega)] + \theta\left(\dfrac{\tau_{st}}{\tau_e}\right)[V_p F_{RS}(\omega) - V_p F_L(\omega)]}{(1+\theta)}. \tag{F34}$$

Equations (F33) and (F34) show that above threshold the noise associated with carrier injection into the active region is not suppressed (since $\theta \ll 1$). Above threshold, the carrier density in the quantum wells is strongly damped and only the carrier density in the SCH region provides negative feedback to suppress the noise associated with carrier injection. Below threshold, the carrier injection noise is suppressed (since $\theta' \approx 1$). Below threshold, the carrier densities in both the SCH region and the quantum wells provide feedback to suppress the carrier injection noise. The spectral density $K_I(\omega)$ of the current noise $\delta I(\omega)$ follows from Eqs. (F33) and (F34),

$$K_I(\omega)|_{\omega < \omega_{3\,\text{dB}}} = \begin{cases} qI & (I < I_{th}) \\[2ex] qI + 2q\,I_{th}\dfrac{(\theta'-\theta)}{(1+\theta)} + 2qn_{sp}\,\eta_i\,(I - I_{th})\dfrac{\left(\theta\dfrac{\tau_{st}}{\tau_e}\right)^2}{(1+\theta)^2} & (I > I_{th}). \end{cases} \tag{F35}$$

In the limit $\omega \to \infty$, the current noise is just the noise associated with carrier injection into the active region and has the spectral density

$$K_I(\omega)|_{\omega \to \infty} = \begin{cases} qI(1+2\,\theta') & (I < I_{th}) \\ qI(1+2\,\theta) + 2q\,I_{th}\,(\theta'-\theta) & (I > I_{th}). \end{cases} \tag{F36}$$

5. Suppression of the current noise by large external impedance

The current noise $\delta I_{ext}(\omega)$ in the external circuit in the presence of an external impedance $Z_s(\omega)$ and an external voltage noise source $\delta V_s(\omega)$ is (Fig. 25)

$$\delta I_{ext}(\omega) = \frac{\delta V_s(\omega)}{[Z(\omega) + Z_s(\omega)]} + \frac{Z(\omega)}{[Z(\omega) + Z_s(\omega)]}\,\delta I(\omega), \tag{F37}$$

where $Z(\omega)$ is the differential impedance of the active region and $Z(\omega = 0) = R_d$. The external impedance $Z_s(\omega)$ is the Thevenin equivalent of the external circuit impedance and the impedance associated with the laser parasitics (ohmic contact resistance, depletion layer capacitance etc.). Assuming that $\delta V_s(\omega)$ represents only the thermal noise originating in $Z_s(\omega)$, the spectral density $K_{I_{ext}}(\omega)$ of the current noise in the external circuit becomes

$$\begin{aligned} K_{I_{ext}}(\omega) &= \frac{K_{V_s}(\omega)}{|Z(\omega) + Z_s(\omega)|^2} + \left|\frac{Z(\omega)}{Z(\omega) + Z_s(\omega)}\right|^2 K_I(\omega) \\[2ex] &= \frac{2K_B T\,\text{Re}\{Z_s(\omega)\}}{|Z(\omega) + Z_s(\omega)|^2} + \left|\frac{Z(\omega)}{Z(\omega) + Z_s(\omega)}\right|^2 K_I(\omega). \end{aligned} \tag{F38}$$

When $Z_s(\omega)$ is much larger than the differential impedance $Z(\omega)$ of the active region then the current noise in the external circuit is just the thermal noise originating in the impedance $Z_s(\omega)$. When $Z_s(\omega)$ is much smaller than $Z(\omega)$ then the current noise in the external circuit is the noise originating inside the active region. By making the impedance $Z_s(\omega)$ very large the current noise in the external circuit can be suppressed well below the shot noise value.

6. Intensity noise

Above threshold, and for frequencies less than $\omega_{3\,\text{dB}}$, $\delta P_{out}(\omega)$ is

$$\begin{aligned} \delta P_{out}(\omega) = {}& \eta_o \eta_i h\nu\frac{I_{ext}(\omega)}{q} + \eta_o h\nu\{(1-\eta_i)[V_c F_c(\omega) \\ & - V_w F_e(\omega)] - \eta_i V_c F_l(\omega) - V_w F_{nr}(\omega) \\ & - V_w F_{RN}(\omega) + \gamma\tau_{st}[V_p F_{RS}(\omega) - V_p F_L(\omega)]\} \\ & + F_o(\omega). \end{aligned} \tag{F39}$$

High-impedance suppression of the current noise $\delta I_{ext}(\omega)$ in the external circuit can have a profound effect on the laser intensity noise through the first term on the right-hand side of the above equation. If $\delta I_{ext}(\omega)$ is suppressed then the spectral density $K_P(\omega)$ of the intensity noise, for frequencies less than $\omega_{3\,\text{dB}}$, is

$$\begin{aligned} K_P(\omega)|_{\omega < \omega_{3\,\text{dB}}} = {}& h\nu P_{out}\left[1 - \eta_o + 2\,\eta_o n_{sp}\left(\frac{1}{\tau_w} + \frac{1-\eta_i}{\tau_e}\right)^2 \tau_{st}^2\right] \\ & + (\eta_o h\nu)^2\left[\eta_i(1-\eta_i)\frac{I}{q} + \eta_i\frac{I_{th}}{q}\right]. \end{aligned} \tag{F40}$$

The low frequency Fano factor of the intensity noise at large bias currents becomes

$$F_P(\omega)\big|_{(\omega<\omega_{3\,\mathrm{dB}},I\gg I_{th})}=1-\eta_o\eta_i. \qquad (F41)$$

In diode lasers both η_o and η_i have typical values around 0.85, and therefore high-impedance suppression of the current noise in the external circuit can result in more than 5-dB suppression of the laser intensity noise below the shot noise value. On the other hand, if the external impedance $Z_s(\omega)$ is much smaller than the impedance $Z(\omega)$ of the active region then it can be shown that at large bias currents the Fano factor of the laser intensity noise approaches unity

$$F_P(\omega)\big|_{(\omega<\omega_{3\,\mathrm{dB}},I\gg I_{th})}=1. \qquad (F42)$$

In practice it is difficult to make $Z_s(\omega)$ very small. One way of obtaining a small external impedance $Z_s(\omega)$ is by using the circuit B shown in Fig.7 and shorting the rf port of the bias T. At frequencies of interest $Z_s(\omega)$ would then just be the parasitic impedance associated with the laser device and would be dominated by the resistance of the device ohmic contacts.

[1] Y.M. Blanter and M. Buttiker, Phys. Rev. B **59**, 10 217 (1999).

[2] J.H. Davies, P. Hyldgaard, Selman Hershfield, and J.W. Williams, Phys. Rev. B **46**, 9620 (1992).

[3] G. Iannaccone, M. Macucci, and B. Pellegrini, Phys. Rev. B **55**, 4539 (1997).

[4] Y. Yamamoto, S. Machida, Phys. Rev. A **35**, 5114 (1987).

[5] F. Rana, R. Ram, Appl. Phys. Lett. **76**, 1083 (2000).

[6] F. Rana, S. G. Patterson, and R. J. Ram, in *Proceedings of the Integrated Photonics Research 1999 Digest*, (OSA Technical Digest Series, Washington, DC, 1999).

[7] J. Faist, F. Capasso, C. Sirtori, D.L. Sivco, A.L. Hutchinson, and A.Y. Cho, Appl. Phys. Lett. **66**, 538 (1995).

[8] J. Faist, F. Capasso, C. Sirtori, D.L. Sivco, A.L. Hutchinson, and A.Y. Cho, Appl. Phys. Lett. **67**, 3057 (1995).

[9] C. Sirtori, J. Faist, F. Capasso, D.L. Sivco, A.L. Hutchinson, S.N.G. Chu, and A.Y. Cho, Appl. Phys. Lett. **68**, 1745 (1996).

[10] C. Sirtori, J. Faist, F. Capasso, D.L. Sivco, A.L. Hutchinson, and A.Y. Cho, IEEE J. Quantum Electron. **33**, 89 (1997).

[11] J. Faist, A. Tredicucci, F. Capasso, C. Sirtori, D.L. Sivco, J.N. Baillargeon, and A.L. Hutchinson, IEEE J. Quantum Electron. **34**, 336 (1998).

[12] C. Sirtori, P. Kruck, S. Barbieri, P. Collot, and J. Nagle, Appl. Phys. Lett. **73**, 3486 (1998).

[13] C. Gmachl, J. Faist, F. Capasso, C. Sirtori, D.L. Sivco, and A.Y. Cho, IEEE J. Quantum Electron. **33**, 1567 (1997).

[14] C. Gmachl, F. Capasso, A. Tredicucci, and D.L. Sivco, Appl. Phys. Lett. **73**, 3830 (1998).

[15] C. Gmachl, F. Capasso, J. Faist, A.L. Hutchinson, A. Tredicucci, D.L. Sivco, J.N. Baillargeon, S.N.G. Chu, and A.Y. Cho, Appl. Phys. Lett. **72**, 1430 (1998).

[16] A. Tredicucci, F. Capasso, C. Gmachl, D.L. Sivco, A.L. Hutchinson, A.Y. Cho, J. Faist, and G. Scamarcio, Appl. Phys. Lett. **72**, 2388 (1998).

[17] A. Tredicucci, F. Capasso, C. Gmachl, D.L. Sivco, A.L. Hutchinson, and A.Y. Cho, Appl. Phys. Lett. **73**, 2101 (1998).

[18] A. Tredicucci, C. Gmachl, F. Capasso, D.L. Sivco, A.L. Hutchinson, A.Y. Cho, J. Faist, and G. Scamarcio, Appl. Phys. Lett. **74**, 638 (1999).

[19] G. Strasser, S. Gianordoli, L. Hvozdara, W. Schrenk, K. Unterrainer, and E. Gornik, Appl. Phys. Lett. **75**, 1345 (1999).

[20] J. Faist, F. Capasso, C. Sirtori, D.L. Sivco, A.L. Hutchinson, and A.Y. Cho, Nature (London) **387**, 777 (1997).

[21] L. A. Coldren and S. Corzine, *Diode Lasers and Photonic Integrated Circuits* (Wiley, New York, 1995).

[22] J. Faist, F. Capasso, C. Sirtori, D.L. Sivco, D.L. Hutchinson, M.S. Hybertsen, and A.Y. Cho, Phys. Rev. Lett. **76**, 411 (1996).

[23] C. Gmachl, F. Capasso, A. Tredicucci, D.L. Sivco, R. Kohler, A.L. Hutchinson, and A.Y. Cho, IEEE J. Sel. Top. Quantum Electron. **5**, 808 (1999).

[24] A. Wacker and A-P. Jauho, Phys. Scr., T **T69**, 321 (1997).

[25] C. W. Gardiner, *Handbook of Stochastic Methods* (Springer-Verlag, New York, 1996).

[26] F. Rana and R. J. Ram, in *Proceedings of the IEEE LEOS Annual Meeting, 1999*, (IEEE Press, Piscataway, NJ, 1999).

[27] P.D. Yoder, K. Gartner, and W. Fichtner, J. Appl. Phys. **79**, 1951 (1996).

[28] It is assumed that $P_{out}(t)=P_{out}+\mathrm{Re}\{\delta P_{out}(\omega)e^{j\omega t}\}$ and $I_{ext}(t)=I+\mathrm{Re}\{\delta I_{ext}(\omega)e^{j\omega t}\}$.

[29] N. Mustafa, L. Pesquera, L. Cheung, and K.A. Shore, IEEE Photonics Technol. Lett. **11**, 527 (1999).

[30] S. Inoue, H. Ohzu, S. Machida, and Y. Yamamoto, Phys. Rev. A **46**, 2757 (1992).

[31] F. Rana, P. Mayer, and R. Ram, in *Proceedings of IEEE LEOS Summer Topical' Conference on Advanced Semiconductor Lasers 2001 (IEEE Press, New Jersey, 2001)*

[32] J. Kim, and Y. Yamamoto, Phys. Rev. B **55**, 9949 (1997).

[33] G. P. Agrawal and N. K. Datta, *Long Wavelength Semiconductor Lasers* (Van Nostrand Reinhold, New York, 1993).

[34] K. Y. Lau, in *Quantum Well Lasers*, edited by P. S. Zory (Academic, New York, 1993).